

# Exploring New Physics in transition $b \rightarrow s \ell^+ \ell^-$ through different $B_c \rightarrow D_s^{(*)} \ell^+ \ell^-$ observables

Qazi Maaz Us Salam<sup>a,b</sup>, Ishtiaq Ahmed<sup>b</sup>, Rizwan Khalid<sup>a</sup>, Ibad Ur Rehman<sup>c</sup>

<sup>a</sup>*School of Science and Engineering, Lahore University of Management Sciences (LUMS), Opposite Sector U, D.H.A, Lahore 54792, Pakistan.*

<sup>b</sup>*National Center for Physics, Islamabad 44000, Pakistan.*

<sup>c</sup>*School Education and Literacy Department, Government of Sindh, Pakistan.*

*E-mail:* [20120011@lums.edu.pk](mailto:20120011@lums.edu.pk), [ishtiaq.ahmed@ncp.edu.pk](mailto:ishtiaq.ahmed@ncp.edu.pk),  
[rizwan\\_khalid@lums.edu.pk](mailto:rizwan_khalid@lums.edu.pk), [ibadnustphy@gmail.com](mailto:ibadnustphy@gmail.com)

**ABSTRACT:** Inspired by the intriguing discrepancies observed in the  $b \rightarrow s \ell^+ \ell^-$  neutral current decays, we study the decay channel  $B_c \rightarrow D_s^{(*)} \ell^+ \ell^-$  ( $\ell = \mu, \tau$ ), which is also the same flavor changing neutral current (FCNC) transition at the quark level. In this context, looking for the potential of physics beyond the standard model (SM) can offer compelling results to the decay  $B_c \rightarrow D_s^{(*)} \ell^+ \ell^-$ . For this purpose, we use the helicity formalism for this decay by employing the effective theory approach where the vector and axial vector new physics (NP) operators are present. In this study, we have calculated several observables, such as the branching ratio  $B_r$ , the  $D^*$  helicity fraction  $f_L$ , the lepton forward-backward asymmetry  $A_{FB}$ , and the lepton flavor universality ratio (LFU)  $R_{D_s^{(*)}}^{\tau\mu}$ . In addition, to a complimentary check on the LFU, we also calculate the ratio of different observables  $R_i^{\tau\mu}$  where  $i = A_{FB}, f_L$ . We assume that the NP universal coupling is present for both muons and taus, while the non-universal coupling is only present for muons. Regarding these couplings, we imply the latest global fit to the  $b \rightarrow s \ell^+ \ell^-$  data, which is recently computed in [1]. We give predictions of some of the mentioned observables within the SM and the various NP scenarios. We found that the considered observables are not only sensitive to the NP but also helpful in distinguishing among the different NP scenarios. These results can be tested at LHCb, HL-LHC, and FCC-ee, and therefore, the precise measurements of these observables not only deepen our understanding of the  $b \rightarrow s \ell^+ \ell^-$  process but also provide a complementary check of the status of different NP scenarios.

---

## Contents

<b>1</b>	<b>Introduction</b>	<b>1</b>
<b>2</b>	<b>Theoretical Description</b>	<b>3</b>
2.1	Effective Hamiltonian and Decay Amplitude of $B_c \rightarrow D_s^* \ell^+ \ell^-$	4
2.2	Matrix Element and Form Factors	5
2.3	Helicity Amplitude of $B_c \rightarrow D_s^* \ell^+ \ell^-$	5
2.3.1	Differential Decay Rate	7
2.4	Forward Backward Asymmetry	7
2.5	Helicity Fraction	7
2.6	Differential decay rate of $B_c \rightarrow D_s \ell^+ \ell^-$	8
2.7	Lepton Flavor Universality (LFU) Ratios	9
<b>3</b>	<b>Phenomenological Analysis</b>	<b>9</b>
3.1	Input Parameters	9
3.2	NP Scenarios	10
3.3	Analysis of the Physical Observables in $B_c \rightarrow D_s^{(*)} \ell^+ \ell^-$ process	13
3.3.1	1D NP scenarios	14
3.3.2	D>1 NP scenarios	17
3.3.3	$B_c \rightarrow D_s \ell^+ \ell^-$ in the presence of 1D and D > 1 NP scenarios	24
<b>4</b>	<b>Summary and Conclusion</b>	<b>26</b>

---

## 1 Introduction

The flavor changing neutral current (FCNC) processes based on the  $b \rightarrow s \ell^+ \ell^-$  transitions in the SM are forbidden at the tree level and occur at the loop level. Due to this fact, any new particles predicted by an extension of the SM can manifest themselves in the loop and consequently effect the value of the observables. Therefore, the FCNC process is an attractive experimental and theoretical topic for testing the SM and checking the possible NP [2, 3].

In this context, the FCNC decay process, particularly,  $B \rightarrow K^{(*)} \ell^+ \ell^-$  has been widely experimentally investigated [4–21]. On the same footing, LHCb collaborations and Belle also reported important data on the  $b \rightarrow d \ell^+ \ell^-$  decay channels such as  $B \rightarrow (\rho, \omega, \pi, \eta) \ell^+ \ell^-$ ,  $B_s^0 \rightarrow \bar{K}^{*0} \mu^+ \mu^-$  and also the ratio between some decay channels belong to the  $b \rightarrow d$  and  $b \rightarrow s$  transitions [22–26]. In relation to this, previously, LFU ratios  $R_K$  and  $R_{K^*}$  measured at LHCb indicated deviations from their SM values even with including the quantum electrodynamic (QED) corrections [18, 20, 27, 28]. Recently, these ratios are aligned with the SM values, resulting in the absence of any LFU violation (LFUV) type

NP [27, 29]. However, branching ratios of decays like  $B \rightarrow K^{(*)}\mu^+\mu^-$ ,  $B_s \rightarrow \phi\mu^+\mu^-$  [19, 30, 31], and also of  $B \rightarrow K^*\mu^+\mu^-$  angular observables, particularly, in  $P'_5$  [32, 33] in different momentum transfer ( $q^2$ ) bins still have considerable sigma deviation with their SM values[1]. For the details about the anomalies, one can consult the book [34] and the review article [3] and the references therein. Moreover, the measurements of  $R_{K_s^0}$  and  $R_{K^{*+}}$  show some deviations from the SM [20, 35, 36]. In addition,  $B_s$  semi-leptonic decays,  $B_s \rightarrow \phi\ell^+\ell^-$  is measured at DØ, CDF and at LHCb collaborations [37–42] and LHCb also reported the  $B_s \rightarrow f'\ell^+\ell^-$  decay process [31].

Similarly, in the last decades, the FCNC  $b \rightarrow s\ell^+\ell^-$  process has also been studied theoretically in detail within the SM [43–65], and to address the above mentioned deviations from the SM that occurred in these FCNC process, they are also studied in the various SM extensions [66–92]. Even though significant progress in the domain of  $B_{d,s}$  rare semileptonic decays has been made both experimentally and theoretically, but a single uniform framework of NP is yet to be determined to address all discrepancies in the current data. These circumstances lead to the motivation to study more decay channels that belong to the same FCNC transition, which may not only provide a complimentary check to the anomalies but also further explore the properties of FCNC transition. Concerning this, different complementary channels have been theoretically explored, such as  $B \rightarrow (K_1, K_2)\mu^+\mu^-$  and  $B_s \rightarrow f'_1\mu^+\mu^-$  in the different NP scenarios [93–96]. Furthermore, on the same footing, the semi leptonic decays of the  $B_c$  meson, particularly  $B_c \rightarrow D_s^{(*)}\ell^+\ell^-$ , can also be a good candidate to test the SM aspects of  $b \rightarrow s\ell^+\ell^-$  transitions as well as to serve as an ideal tool to probe any possible NP in the FCNC sector.

With regard to this, in comparison to the  $B_s$  mesons, the  $B_c$  meson is less explored both theoretically and experimentally. As previously, LHCb collaborations found that the fragmentation of the  $B_c$  meson,  $f_u$ , is approximately a thousand times smaller than the fragmentation of  $B_u$  meson,  $f_b$  [97], resulting in less experimental interest. However, recently, LHCb collaborations set an upper limit for the decay channel  $B_c^+ \rightarrow D^+\ell^+\ell^-$  as  $\frac{f_u}{f_c} \times \mathcal{B}_r(B_c^+ \rightarrow D^+\ell^+\ell^-) < 9.6 \times 10^{-8}$  [98]. Although the branching ratios of  $B_c \rightarrow D_s^{(*)}\ell^+\ell^-$  have the same order [99] but due to the reconstruction of  $D_s^* \rightarrow D\pi$  makes this decay channel more difficult to measure at LHCb with the current luminosity. Despite that, at future colliders such as high luminosity LHCb (HL-LHCb) and the future circular collider (FCC-ee), the situation will be improved, and the measurement of the semi leptonic  $B_c$  meson decays might be possible.

From a theoretical perspective, the  $B_c$  rare semileptonic decays,  $B_c^+ \rightarrow D^+\ell^+\ell^-$ , are studied using several approaches, such as the relativistic quark model, the light-front quark model, the QCD sum rule etc [99–103]. From the NP point of this decay, channels are studied in various extensions of SM such as single Universal extra dimension, non-Universal  $Z'$ , Two Higgs Doublet Models, and recently using the model-independent approach [95, 104–111]. With the same motivation, it is interesting to check the potential of physics beyond the SM in decay  $B_c \rightarrow D_s^{(*)}\ell^+\ell^-$  ( $\ell = \mu, \tau$ ). For this purpose, we use the helicity formalism for this decay by employing the effective theory approach where the vector and axial vector NP operators are present. In this study, we have calculated several observables, such as the branching ratio  $\mathcal{B}_r$ , the  $f_L$ , the  $A_{FB}$ , and the LFU  $R_{D_s^*}^{\tau\mu}$ .

In addition, to a complementary check on the LFU, we also calculate the ratio of different observables  $R_i^{\tau\mu}$  where  $i = A_{FB}, f_L$ . It is necessary to emphasize here that the authors of [111] study  $B_c \rightarrow D_s^{(*)} \ell^+ \ell^-$  only within the NP scenarios where the couplings to the leptons are universal. However, in the current study, we assume that the NP universal coupling is present for both muons and taus, while the non-universal coupling is only present for muons. Regarding these couplings, we imply the latest global fit to the  $b \rightarrow s \ell^+ \ell^-$  data, which is recently computed in [1]. Furthermore, to check the sensitivity of the NP couplings to the observable as a function of  $q^2$ , we set them by optimizing within their  $1\sigma$  ranges, which give the maximum and minimum deviation from their SM values. Moreover, we have also calculated the maximum and minimum variation after the integration over the low  $q^2$  bin for  $\mu$  and high  $q^2$  bin for both  $\mu$  and  $\tau$ . Besides, to see the explicit dependence on the couplings, we have calculated the analytical expressions of these observables in terms of NP Wilson coefficients (WCs) and plotted them against the NP couplings in their  $1\sigma$  range, which is very useful for determining the precise values of the universal and non-universal couplings in the future.

For the calculations, we use FeynCalc and Mathematica to solve the hadronic and leptonic parts, their traces appearing in the analytical expressions, and to get the numerical values of the observables. We give our predictions of the mentioned observables both for  $\mu$  and  $\tau$  leptons within the SM and the various NP scenarios where it is found that the considered observables are not only sensitive to the NP but also helpful in distinguishing among the different NP scenarios. It is also important to mention here that the tau pair mode is less studied, for instance, recently studied in  $B^0 \rightarrow K^{*0} \tau^+ \tau^-$  [112] and the Belle experiment also sets the upper limit of the branching fraction  $< 3.1 \times 10^{-3}$  at a 90% confidence level [12] which is still approximately some order smaller than the branching ratio. However, the situation will improve in high luminosity LHCb (HL-LHCb) and FCC-ee, where these results can be tested. Therefore, the precise measurements of these observables not only deepen our understanding of the  $b \rightarrow s \ell^+ \ell^-$  process, but also provide a complementary check of the status of different NP scenarios.

This paper is structured as follows. In §2, we set the complete theoretical description required for the  $B_c \rightarrow D_s^* \ell^+ \ell^-$  decays. In this section, we have given the parameterization of  $B_c \rightarrow D_s^*$  hadronic matrix elements in terms of the seven form factors, the helicity formalism, the formulae of the branching ratio, the forward-backward asymmetry, the helicity fraction, and the lepton flavor ratio. In §3, we have given the values of various parameters and the form factors (which are calculated in the relativistic quark model) and the values of different NP scenarios in  $1\sigma$  region. We have also discussed the phenomenology of the observables considered in the presence of different NP scenarios. In the last section, §4, we describe the summary and the conclusion of our work.

## 2 Theoretical Description

In this section, we provide the theoretical formulation which require to calculate the helicity amplitude of  $B_c \rightarrow D_s^* \ell^+ \ell^-$  meson decays. After that, we write the differential decay rate

in terms of helicity amplitude, and further, we extend our framework to observables such as  $A_{FB}$ ,  $f_L$ , and  $R_{D_s^{(*)}}$ .

## 2.1 Effective Hamiltonian and Decay Amplitude of $B_c \rightarrow D_s^* \ell^+ \ell^-$

We calculate exclusive semileptonic  $B_c$  meson decay  $B_c \rightarrow D_s^* \ell^+ \ell^-$  with in SM and beyond. The quark level Feynman diagram for this process is shown in Fig.1.

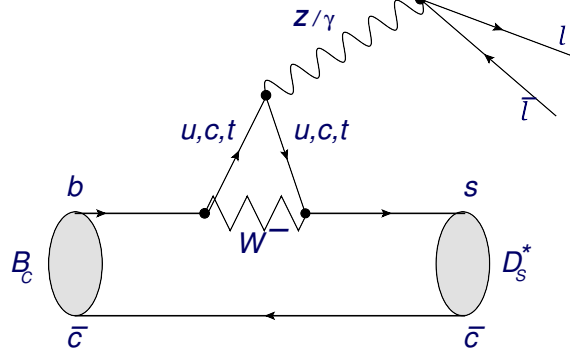


**Figure 1.** Penguin diagram for  $B_c \rightarrow D_s^* \ell^+ \ell^-$  decay

The Amplitude for  $B_c \rightarrow D_s^* \ell^+ \ell^-$  which is based on quark level transition of  $b \rightarrow s \ell^+ \ell^-$  decay can be written as follow;

$$\begin{aligned}
\mathcal{M} = & -\frac{G_F \alpha}{\sqrt{2} \pi} V_{tb} V_{ts}^* \{ \mathcal{C}_9^{\text{eff}} \langle D_s^*(k, \epsilon) | \bar{s} \gamma_\mu P_L b | B_c(p) \rangle \langle \bar{l} \gamma^\mu l \rangle + \mathcal{C}_{10}^{\text{eff}} \langle D_s^*(k, \epsilon) | (\bar{s} \gamma_\mu P_L b) | B_c(p) \rangle \langle \bar{l} \gamma^\mu \gamma^5 l \rangle \\
& - 2 \mathcal{C}_7^{\text{eff}} \frac{m_b}{q^2} \langle D_s^*(k, \epsilon) | (\bar{s} i \sigma_{\mu\nu} q^\nu P_R b) | B_c(p) \rangle \langle \bar{l} \gamma^\mu l \rangle \\
& + \mathcal{C}_{9\ell} \langle D_s^*(k, \epsilon) | \bar{s} \gamma_\mu P_L b | B_c(p) \rangle \langle \bar{l} \gamma^\mu l \rangle + \mathcal{C}_{10\ell} \langle D_s^*(k, \epsilon) | (\bar{s} \gamma_\mu P_L b) | B_c(p) \rangle \langle \bar{l} \gamma^\mu \gamma^5 l \rangle \\
& + \mathcal{C}'_{9\ell} \langle D_s^*(k, \epsilon) | \bar{s} \gamma_\mu P_R b | B_c(p) \rangle \langle \bar{l} \gamma^\mu l \rangle + \mathcal{C}'_{10\ell} \langle D_s^*(k, \epsilon) | (\bar{s} \gamma_\mu P_R b) | B_c(p) \rangle \langle \bar{l} \gamma^\mu \gamma^5 l \rangle \}.
\end{aligned} \tag{2.1}$$

Here,  $P_{L,R} = \frac{1}{2}(1 \mp \gamma_5)$

## 2.2 Matrix Element and Form Factors

The matrix elements appeared in Eq. (2.1) can be parameterized in terms of form factors which are the scalar functions of the square of the momentum transfer  $q^2 = (p - k)^2$ .

$$\begin{aligned}
\langle D_s^*(k, \epsilon) | \bar{s} \gamma_\mu b | B_c(p) \rangle &= \frac{2i\epsilon_{\mu\nu\alpha\beta}}{M_{B_c} + M_{D_s^*}} \epsilon^{*\nu} p^\alpha k^\beta A_V(q^2) \\
\langle D_s^*(k, \epsilon) | \bar{s} \gamma_\mu \gamma_5 b | B_c(p) \rangle &= (M_{B_c} + M_{D_s^*}) \epsilon^{*\mu} A_0(q^2) - \frac{(\epsilon^* \cdot q) A_+(q^2)}{M_{B_c} + M_{D_s^*}} (p + k)^\mu \\
&\quad - \frac{A_-(q^2)}{M_{B_c} + M_{D_s^*}} (\epsilon^* \cdot q) q^\mu \\
\langle D_s^*(k, \epsilon) | \bar{s} i \sigma_{\mu\nu} q^\nu b | B_c(p) \rangle &= 2i\epsilon_{\mu\nu\alpha\beta} \epsilon^{*\nu} p^\alpha k^\beta T_1(q^2) \\
\langle D_s^*(k, \epsilon) | \bar{s} i \sigma_{\mu\nu} q^\nu \gamma^5 b | B_c(p) \rangle &= \left[ (M_{B_c}^2 + M_{D_s^*}^2) \epsilon_\mu^* - (\epsilon^* \cdot q)(p + k)_\mu \right] T_2(q^2) \\
&\quad + (\epsilon^* \cdot q) \left[ q_\mu - \frac{q^2}{(M_{B_c}^2 + M_{D_s^*}^2)} (p + k)_\mu \right] T_3(q^2) \quad (2.2)
\end{aligned}$$

where  $p$  denotes the momentum of  $B_c$  meson and  $\epsilon(k)$  are the polarization vector of  $D_s^*$  meson. The  $A_V(q^2)$ ,  $A_0(q^2)$ ,  $A_+(q^2)$ ,  $A_-(q^2)$ ,  $T_1(q^2)$ ,  $T_2(q^2)$  and  $T_3(q^2)$  are the seven independent form factors.

## 2.3 Helicity Amplitude of $B_c \rightarrow D_s^* \ell^+ \ell^-$

Before to examine the various observables, it is convenient to use the amplitude in a helicity basis. To achieve this, first we can write the amplitude by substituting the matrix elements defined in Eq. 2.1, in the following form

$$\mathcal{M} = -\frac{G_F \alpha}{2\sqrt{2}\pi} V_{tb} V_{ts}^* [T_\mu^1 (\bar{l} \gamma^\mu l) + T_\mu^2 (\bar{l} \gamma^\mu \gamma^5 l)] \quad (2.3)$$

where,

$$\begin{aligned}
T_\mu^1 &= -i\epsilon_{\mu\nu\alpha\beta} \epsilon^{*\nu} p^\alpha k^\beta \mathcal{F}_1(q^2) - g_{\mu\nu} \mathcal{F}_2(q^2) + q_\mu q_\nu \mathcal{F}_3(q^2) + P_\mu q_\nu \mathcal{F}_4(q^2) \\
T_\mu^2 &= -i\epsilon_{\mu\nu\alpha\beta} \epsilon^{*\nu} p^\alpha k^\beta \mathcal{F}_5(q^2) - g_{\mu\nu} \mathcal{F}_6(q^2) + q_\mu q_\nu \mathcal{F}_7(q^2) + P_\mu q_\nu \mathcal{F}_8(q^2)
\end{aligned}$$

The functions  $\mathcal{F}_1$  to  $\mathcal{F}_8$  in Eq. 2.4 are recognized as auxiliary functions. Auxiliary functions contain both SD (Wilson coefficients (WCs)) and LD (Form factors).

We write the auxiliary functions as follows;

$$\begin{aligned}
\mathcal{F}_1 &= \frac{2C_9^{\text{eff}} A_V(q^2)}{M_{D_s^*} + M_{B_c}} + \frac{4m_b}{q^2} C_7^{\text{eff}} T_1(q^2), \\
\mathcal{F}_2 &= C_9^{\text{eff}} A_0(q^2) (M_{D_s^*} + M_{B_c}) + \frac{2m_b}{q^2} C_7^{\text{eff}} T_2(q^2) (M_{D_s^*} + M_{B_c}), \\
\mathcal{F}_3 &= \frac{A_-(q^2) C_9^{\text{eff}}}{M_{D_s^*} + M_{B_c}} + \frac{2m_b}{q^2} C_7^{\text{eff}} T_3(q^2), \quad \mathcal{F}_4 = \frac{A_+(q^2) C_9^{\text{eff}}}{M_{D_s^*} + M_{B_c}} + \frac{2m_b}{q^2} (T_2(q^2) + \frac{q^2 T_3(q^2)}{M_{D_s^*} + M_{B_c}}), \\
\mathcal{F}_5 &= \frac{2C_{10}^{\text{eff}} A_V(q^2)}{M_{D_s^*} + M_{B_c}}, \quad \mathcal{F}_6 = C_{10}^{\text{eff}} (M_{D_s^*} + M_{B_c}) A_0(q^2), \quad \mathcal{F}_7 = \frac{C_{10}^{\text{eff}} A_-(q^2)}{M_{D_s^*} + M_{B_c}}, \\
\mathcal{F}_8 &= \frac{C_{10}^{\text{eff}} A_+(q^2)}{M_{D_s^*} + M_{B_c}}. \quad (2.4)
\end{aligned}$$

The hadronic tensor in terms of helicity basis  $\varepsilon^{\dagger\mu}(m)$  [113] can be written as,

$$H_m^i = \varepsilon^{\dagger\mu}(m) T_\mu^{(i)}, \quad H_m^i = \varepsilon^{\dagger\mu}(m) \varepsilon^{\dagger\nu}(n) T_{\mu\nu}^{(i)}. \quad (2.5)$$

Where  $T_\mu^{(i)} = \varepsilon^{\dagger\nu}(n) T_{\mu\nu}^{(i)}$ ,  $\varepsilon^\nu$  is the vector polarization of the final state  $D_s^*$  meson:  $m, n = 0, \pm, t$ , are the longitudinal, transverse and time components, where  $i = 1, 2$ . The helicity components of the polarization vector read as:  $\epsilon^\mu(\pm) = \frac{1}{\sqrt{2}}(0, \pm 1, i, 0)$ ,  $\epsilon^\mu(0) = \frac{1}{m}(|k|, 0, 0, E)$ , and  $g_{mn} = \text{diagonal}(+, -, -, -)$ . The Kinematic for  $B$ -meson in the rest frame is  $p^\mu = (m_B, 0, 0, 0)$ ,  $k^\mu = (E_k, 0, 0, |k|)$ , and  $q^\mu = (q_0, 0, 0, |k|)$ . Now, the polarization vectors read as

$$\varepsilon^\mu(t) = \frac{1}{\sqrt{q^2}}(q_0, 0, 0, |k|), \quad \varepsilon^\mu(\pm) = \frac{1}{\sqrt{2}}(0, \mp 1, i, |k|), \quad \varepsilon^\mu(0) = \frac{1}{\sqrt{q^2}}(|k|, 0, 0, q_0)$$

where,  $|k| = \frac{\sqrt{\lambda}}{2m_B}$ ;  $\lambda = m_B^4 + m_{D_s^*}^4 + q^4 - 2(m_B^2 m_{D_s^*}^2 + m_{D_s^*}^2 q^2 + m_B^2 q^2)$  and  $E_{D_s^*} = \frac{m_B^2 + m_{D_s^*}^2 - q^2}{2m_B}$ ,  $D_s^*$  is final state meson, so using equation of Hadronic tensor we have,

$$\begin{aligned} H_0^{(1)} &= \frac{1}{m_{D_s^*} \sqrt{q^2}} [2q_0 |k|^2 (q_0 - E_{D_s^*}) \mathcal{F}_2 + (|k|^2 + q_0 E_{D_s^*}) \mathcal{F}_3 \\ &\quad + |k|^2 (q_0 (m_B + 2E_{D_s^*}) - q_0^2 - E_{D_s^*} (m_B + E_{D_s^*})) \mathcal{F}_4], \\ H_0^{(2)} &= \frac{1}{m_{D_s^*} \sqrt{q^2}} [2q_0 |k|^2 (q_0 - E_{D_s^*}) \mathcal{F}_6 + (|k|^2 + q_0 E_{D_s^*}) \mathcal{F}_7 \\ &\quad + |k|^2 (q_0 (m_B + 2E_{D_s^*}) - q_0^2 - E_{D_s^*} (m_B + E_{D_s^*})) \mathcal{F}_8], \\ H_+^{(1)} &= -i|k|m_B \mathcal{F}_1 + \mathcal{F}_3, \quad H_+^{(2)} = -i|k|m_B \mathcal{F}_5 + \mathcal{F}_7, \quad H_-^{(1)} = i|k|m_B \mathcal{F}_1 + \mathcal{F}_3, \\ H_-^{(2)} &= i|k|m_B \mathcal{F}_5 + \mathcal{F}_7. \end{aligned} \quad (2.6)$$

These are the components of the hadronic tensor. The subscripts  $\pm, 0$  denote the transverse and longitudinal helicity components. We have ignored the time component for both leptonic and hadronic tensors. For the leptonic tensors  $L_{\mu\nu}^{(k)}$  in  $\bar{l}l$  center of mass frame (COM), we can write,  $q^\mu = (\sqrt{q^2}, \vec{0})$ ,  $p_1^\mu = (E_l, |p_1| \sin \theta, 0, |p_1| \cos \theta)$ , and  $p_2^\mu = (E_l, -|p_1| \sin \theta, 0, -|p_1| \cos \theta)$  with  $E_l = \sqrt{q^2}/2$  and  $|p_1| = \sqrt{q^2 - 4m_l^2}/2$  and the polarization vectors in  $\bar{l}l$  COM frame are:  $\epsilon^\mu(\pm) = \frac{1}{\sqrt{2}}(0, \pm 1, i, 0)$ ,  $\epsilon^\mu(0) = (0, 0, 0, 1)$ , and  $\epsilon^\mu(t) = (1, 0, 0, 0)$ . Hence, by using these information of polarization of vectors and lepton kinematics, we have calculated lepton tensor components and by using these leptonic tensor components plus the hadronic tensor components, now we can write amplitude of decay  $B_c \rightarrow D_s^* \ell^+ \ell^-$  in terms of helicity basis, mentioned in Eq 2.9.

### 2.3.1 Differential Decay Rate

We write the branching ratio in terms of helicity amplitude, which is:

$$\frac{d^2\Gamma(B_c \rightarrow D_s^* \ell^+ \ell^-)}{dq^2} = \frac{1}{(2\pi)^3} \frac{1}{32M_{B_c}^3} \int_{+(q^2)}^{-(q^2)} dq^2 |\mathcal{M}|^2. \quad (2.7)$$

$$\begin{aligned} \frac{d^2\Gamma(B_c \rightarrow D_s^* \ell^+ \ell^-)}{dq^2 d\cos\theta} &= \frac{G_F^2}{(2\pi)^3} \left( \frac{\alpha|\lambda_t|}{2\pi} \right)^2 \frac{|k| \sqrt{1 - 4m_l^2/q^2}}{8m_l^2} \frac{1}{2} [ L_{\mu\nu}^{(1)} \cdot (H_{11}^{\mu\nu} + H_{22}^{\mu\nu}) \\ &\quad - \frac{1}{2} L_{\mu\nu}^{(2)} (q^2 H_{11}^{\mu\nu} + (q^2 - m_l^2) H_{22}^{\mu\nu}) + L_{\mu\nu}^{(3)} \cdot (H_{12}^{\mu\nu} + H_{21}^{\mu\nu}) ]. \end{aligned} \quad (2.8)$$

Where  $\lambda_t = |V_{ts}^\dagger V_{tb}|$  denotes CKM matrices,  $|k|$  denotes the momentum of vector meson given in the rest frame of  $B$  meson. After integration over  $\cos\theta$  and putting the values of the leptonic and hadronic tensor components  $L^{(k)}(m, n)$ ,  $H^{ij}(m, n)$  respectively, we get

$$\begin{aligned} \frac{d\Gamma(B \rightarrow D_s^* \ell^+ \ell^-)}{dq^2} &= \frac{G_F^2}{(2\pi)^3} \left( \frac{\alpha|\lambda_t|}{2\pi} \right)^2 \frac{\lambda^{1/2} q^2}{48M_B^3} \sqrt{1 - 4m_l^2/q^2} [ H^1 H^{1\dagger} (1 + 4m_l^2/q^2) \\ &\quad + H^2 H^{2\dagger} (1 - 4m_l^2/q^2) ]. \end{aligned} \quad (2.9)$$

Where  $m_l$  denotes as the lepton mass,  $\lambda = M_B^4 + M_{D_s^*}^4 + q^4 - 2(M_B^2 M_{D_s^*}^2 + M_{D_s^*}^2 q^2 + M_B^2 q^2)$  and we separated out transverse and longitudinal hadronic components of amplitudes. Genereally one can define  $H^i H^{i\dagger} \equiv H_+^i H_+^{i\dagger} + H_-^i H_-^{i\dagger} + H_0^i H_0^{i\dagger}$ . Branching ratios are precisely used in literature to find NP effects.

### 2.4 Forward Backward Asymmetry

We determine leptons forward-backward asymmetry ( $\mathcal{A}_{FB}$ ) to analyze our said process. The  $\mathcal{A}_{FB}$  of leptons is defined as;

$$\mathcal{A}_{FB} = \frac{\mathcal{N}^F - \mathcal{N}^B}{\mathcal{N}^F + \mathcal{N}^B}, \quad (2.10)$$

where  $\mathcal{N}^F(\mathcal{N}^B)$  is the number of event in which leptons moving in forward(backward) directions. We use the double differential decay rate formula from Eq. 2.9 to simplify the following expression for forward-backward asymmetries;

$$\mathcal{N}^F = \int_0^1 d\cos\theta \frac{d^2\Gamma(q^2, \cos\theta)}{dq^2 d\cos\theta}, \quad \mathcal{N}^B = \int_{-1}^0 d\cos\theta \frac{d^2\Gamma(q^2, \cos\theta)}{dq^2 d\cos\theta}. \quad (2.11)$$

We write the analytical expression for forward-backward Asymmetry of leptons as follows;

$$A_{FB} = \frac{3}{4} \sqrt{1 - \frac{4m_l^2}{q^2}} \frac{\text{Re}(H_+^{(1)} H_+^{\dagger(2)}) - \text{Re}(H_-^{(1)} H_-^{\dagger(2)})}{H^{(1)} H^{\dagger(1)} (1 + \frac{4m_l^2}{q^2}) + H^{(2)} H^{\dagger(2)} (1 - \frac{4m_l^2}{q^2})}. \quad (2.12)$$

### 2.5 Helicity Fraction

We write a differential expression for longitudinal helicity fraction of  $D_s^*$  meson;

$$f_L = \frac{d\Gamma_L(q^2)/dq^2}{d\Gamma(q^2)/dq^2}, \quad (2.13)$$



where  $d\Gamma_L(q^2)/dq^2$  is the longitudinal component of decay rate. Now we can easily write the following analytical expression for longitudinal helicity fraction by using the longitudinal and total component of decay rate in Eq. 2.13;

$$f_L(q^2) = \frac{H_0^{(1)} H_0^{(1)\dagger} (1 + \frac{4m_l^2}{q^2}) + H_0^{(2)} H_0^{(2)\dagger} (1 - \frac{4m_l^2}{q^2})}{H^{(1)} H^{(1)\dagger} (1 + \frac{4m_l^2}{q^2}) + H^{(2)} H^{(2)\dagger} (1 - \frac{4m_l^2}{q^2})}. \quad (2.14)$$

The longitudinal helicity fraction of  $D_s^*$  meson hints at the influence of NP in  $B_c \rightarrow D_s^* \ell^+ \ell^-$  decays.

## 2.6 Differential decay rate of $B_c \rightarrow D_s \ell^+ \ell^-$

Besides with the vector meson  $D_s^*$  as a final state meson, in the present work, we also give the analysis of the  $B_c \rightarrow D_s \ell^+ \ell^-$  process. The branching ratio of this channel is read as [114]

$$\frac{dBr}{dq^2} = 2a_l + \frac{2c_l}{3}, \quad (2.15)$$

where  $a_l$  and  $c_l$  are defined as

$$\begin{aligned} a_l &= C_l \left[ q^2 |\mathcal{F}_P|^2 + \frac{\lambda}{4} (|\mathcal{F}_A|^2 + |\mathcal{F}_V|^2) + 4m_l^2 M_{B_c}^2 |\mathcal{F}_A|^2 + 2m_l (M_{B_c}^2 - M_{D_s}^2 + q^2) \text{Re}(\mathcal{F}_P \mathcal{F}_A^*) \right], \\ c_l &= -C_l \frac{\lambda}{4} \left( 1 - \frac{4m_l^2}{q^2} \right) (|\mathcal{F}_A|^2 + |\mathcal{F}_V|^2). \end{aligned} \quad (2.16)$$

With

$$C_l = \frac{(\alpha |\lambda_t|)^2}{2^9 \pi^5 M_{B_c}^3} \sqrt{1 - \frac{4m_l^2}{q^2}} \sqrt{\lambda}; \quad \lambda = M_{B_c}^4 + M_{D_s}^4 + q^4 - 2(M_{B_c}^2 M_{D_s}^2 + M_{D_s}^2 q^2 + M_{B_c}^2 q^2)$$

The expressions of the form factors  $\mathcal{F}_P$ ,  $\mathcal{F}_V$ , and  $\mathcal{F}_A$  are provided as

$$\begin{aligned} \mathcal{F}_P &= -m_l (C_{10}^{\text{eff}} + C_{10\ell} + C'_{10\ell}) \left[ f_+ - \frac{M_{B_c}^2 - M_{D_s}^2}{q^2} (f_0 - f_T) \right], \\ \mathcal{F}_V &= (C_9^{\text{eff}} + C_{9\ell} + C'_{9\ell}) f_+ + \frac{2m_b}{M_{B_c} + M_{D_s}} C_7^{\text{eff}} f_T, \\ \mathcal{F}_A &= (C_{10}^{\text{eff}} + C_{10\ell} + C'_{10\ell}) f_+. \end{aligned}$$

It is worth mentioning here that  $D_s$  is a scalar meson, and the  $A_{FB}$  for this channel is zero until unless we include the scalar-type couplings. As in the current study, we have considered only the vector and the axial type NP. Therefore, both observables are absent in the  $B_c \rightarrow D_s \ell^+ \ell^-$  process. However, with the branching ratio, we have studied the LFU ratio in and beyond the SM for this channel, and the formula for this ratio is given in the next section.

## 2.7 Lepton Flavor Universality (LFU) Ratios

Lepton Flavor Universality ratios are the ratio of branching ratios to different lepton generations, and this observable is an ideal tool to test for NP in  $B_c \rightarrow D_s^{(*)} \ell^+ \ell^-$  process. We compare cross sections or decay widths that change only in lepton flavors, like tau and muon. The analytical expression for the LFU ratio can be written as;

$$R_{D_s^{(*)}} = \frac{\int_{q_{min}^2}^{q_{max}^2} \frac{d\mathcal{B}(B_c \rightarrow D_s^{(*)} \tau^+ \tau^-)}{dq^2} dq^2}{\int_{q_{min}^2}^{q_{max}^2} \frac{d\mathcal{B}(B_c \rightarrow D_s^{(*)} \mu^+ \mu^-)}{dq^2} dq^2} \quad (2.17)$$

Deviation in the LFU ratio from the SM predictions is a good sign of the presence of NP.

## 3 Phenomenological Analysis

### 3.1 Input Parameters

We present all the inputs that are used for the analysis of all the decay observables. We use a renormalization scale of  $\mu \sim m_b$  for the entire analysis. Values of various input parameters that operate in the numerical analysis are mentioned in Table 1.

$M_{B_c} = 6.275 \text{ GeV [115]}, M_{D_s^*} = 2.1123 \text{ GeV [115]}, M_{D_s} = 1.968 \text{ GeV [115]}$ $m_b(\overline{\text{MS}}) = 4.2 \text{ GeV [116]}, m_c(\overline{\text{MS}}) = 1.28 \text{ GeV [116]}, m_b(\text{pole}) = 4.8 \text{ GeV [116]},$ $m_e = 0.51099895000 \text{ MeV [115]}, m_\mu = 105.6583755 \text{ MeV [115]}, m_\tau = 1776.93 \text{ MeV [115]},$ $\tau_{B_c} = 0.46 \times 10^{-12} \text{ sec [115]}, \alpha^{-1} = 137.035999 \text{ [115]}, G_F = 1.166378 \times 10^{-5} \text{ GeV}^{-2} \text{ [115]},$ $ V_{tb}V_{ts}^*  = 0.0401 \pm 0.0010 \text{ [117]},$
--

**Table 1.** Numerical values of various input parameters used in numerical analysis.

We use the parameterization of the form factors, which depends on the momentum transfer ( $q^2$ ). the transition for  $B_c \rightarrow D_s^{(*)}$  form factors  $\mathcal{F}(q^2)$  taken from [101].

$$\mathcal{F}(q^2) = \begin{cases} \frac{\mathcal{F}(0)}{\left(1 - \frac{q^2}{M^2}\right) \left(1 - \alpha \frac{q^2}{M_{B_s^{(*)}}^2} + \beta \frac{q^4}{M_{B_s^{(*)}}^4}\right)}, & \text{for } \mathcal{F}(q^2) = \{A_V(q^2), A_0(q^2), T_1(q^2), f_+(q^2), f_T(q^2)\} \\ \frac{\mathcal{F}(0)}{\left(1 - \alpha \frac{q^2}{M_{B_s^{(*)}}^2} + \beta \frac{q^4}{M_{B_s^{(*)}}^4}\right)}, & \text{for } \mathcal{F}(q^2) = \{A_+(q^2), A_-(q^2), T_2(q^2), T_3(q^2), f_0(q^2)\} \end{cases}$$

where the values of  $\mathcal{F}(0)$ ,  $\alpha$  and  $\beta$  are given in Table 2. The  $A_0(q^2)$  form factor contains  $M = M_{B_s}$ , and all other form factors contain  $M = M_{B_s^*}$ . The values of  $M_{B_s} = 5.36692 \text{ GeV [115]}$  and  $M_{B_s^*} = 5.4154 \text{ GeV [115]}$  are used. The hadronization of quarks and gluons is described by the form factors that use QCD in the non-perturbative method and are a vital basis for theoretical uncertainties. To measure the effect of the form factor uncertainties on different observables, we have used  $\pm 5 \%$  uncertainty in  $\mathcal{F}(0)$ ,  $\alpha$ , and  $\beta$  [109].

	$A_V(q^2)$	$A_0(q^2)$	$A_+(q^2)$	$A_-(q^2)$	$T_1(q^2)$	$T_2(q^2)$	$T_3(q^2)$	$f_+(q^2)$	$f_0(q^2)$	$f_T(q^2)$
$\mathcal{F}(0)$	0.182	0.070	0.089	0.110	0.085	0.085	0.051	0.129	0.129	0.098
$\alpha$	2.133	1.561	2.479	2.833	1.540	2.577	2.783	2.096	2.331	1.412
$\beta$	1.183	0.192	1.686	2.167	0.248	1.859	2.170	1.147	1.666	0.048

**Table 2.** Form factors of  $B_c \rightarrow D_s^{(*)}$  decays which are calculated by relativistic quark model [101].

The numerical inputs of Wilson coefficients in the SM, calculated at the renormalization scale  $\mu \sim m_b$  [118], are shown in Table 3.

$C_1$	$C_2$	$C_3$	$C_4$	$C_5$	$C_6$	$C_7$	$C_8$	$C_9$	$C_{10}$
-0.294	1.017	-0.0059	-0.087	0.0004	0.0011	-0.295	-0.163	4.114	-4.193

**Table 3.** Wilson coefficients evaluated NNLL at  $\mu \sim m_b$  renormalizable scale from ref. [118].

### 3.2 NP Scenarios

Our primary purpose is to specify the effect of NP on  $B_c \rightarrow D_s^{(*)} \tau^+ \tau^-$  decay observables. Our study uses an effective theory formalism in the presence of new vector (V) and axial vector (A) couplings. We consider the best-fit data of NP couplings in different scenarios from the current global fit analysis [119]. As mentioned in Eq.(2.1),  $\mathcal{C}_{(9,10)\ell}$  and  $\mathcal{C}'_{(9,10)\ell}$  are the NP Wilson coefficients consisting of universal and non-universal components where ( $\ell = e, \mu, \tau$ ) can be written in the following manner.

$$\begin{aligned} \mathcal{C}_{(9,10)e} &= \mathcal{C}_{(9,10)\tau} = \mathcal{C}_{(9,10)}^U, & \mathcal{C}'_{(9,10)e} &= \mathcal{C}'_{(9,10)\tau} = \mathcal{C}_{(9,10)}^U, \\ \mathcal{C}_{(9,10)\mu} &= \mathcal{C}_{(9,10)}^U + \mathcal{C}_{(9,10)\mu}^V, & \mathcal{C}'_{(9,10)\mu} &= \mathcal{C}_{(9,10)}^U + \mathcal{C}_{(9,10)\mu}^V. \end{aligned} \quad (3.1)$$

$\mathcal{C}_{(9,10)}^U$  and  $\mathcal{C}_{(9,10)}^U$  Wilson coefficients are the universal contributions that equally contribute to  $b \rightarrow s \ell^+ \ell^-$  transitions.  $\mathcal{C}_{(9,10)}^V$  and  $\mathcal{C}_{(9,10)}^V$  Wilson coefficients are non-universal contributions, which only allow for the  $b \rightarrow s \mu^+ \mu^-$  decay. We define two frameworks named F-I and F-II. F-I has condition  $\mathcal{C}_{(9,10)\mu}^V = \mathcal{C}_{(9,10)\mu}^V = 0$ , that allows universal couplings only. F-II has both universal and non-universal couplings. Within F-I, the scenarios S1, S2, and S3 preferred by the recent data and the  $1\sigma$  range of the Wilson coefficients, as mentioned in [119], are grouped in Table 4. A complete set of preferred scenarios S4, S5, S6, S7, S8, S9, S10 and S11 was identified for F-II [120]. These NP scenarios, along with the updated  $1\sigma$  range of the Wilson coefficients, as mentioned in [1], are grouped in Table 5 and Table 6. The Wilson coefficients parameter space is specified as a global fit to 254 observables in  $b \rightarrow s \ell^+ \ell^-$  transition [120].

F-I Solutions	Wilson Coefficients	$1\sigma$ range
S1	$\mathcal{C}_9^U$	$(-1.00, -1.33)$
S2	$\mathcal{C}_9^U = -\mathcal{C}_{10}^U$	$(-0.38, -0.62)$
S3	$\mathcal{C}_9^U = -\mathcal{C}_9^U$	$(-0.72, -1.04)$

**Table 4.** Allowed NP  $1\sigma$  parametric range of  $D = 1$  NP Universal couplings. The S1 scenario is introduced in [1], and the S2 and S3 scenarios are introduced in [119].

F-II Solutions	Wilson Coefficients	$1\sigma$ range
S5	$\mathcal{C}_{9\mu}^V$	(-1.43, -0.61 )
	$\mathcal{C}_{10\mu}^V$	(-0.75, 0.00)
	$\mathcal{C}_9^U = \mathcal{C}_{10}^U$	(-0.16, 0.58)
S6	$\mathcal{C}_{9\mu}^V = -\mathcal{C}_{10\mu}^V$	(-0.34, -0.20)
	$\mathcal{C}_9^U = \mathcal{C}_{10}^U$	(-0.53, -0.29)
S7	$\mathcal{C}_{9\mu}^V$	(-0.39, -0.02)
	$\mathcal{C}_9^U$	(-1.21, -0.72)
S8	$\mathcal{C}_{9\mu}^V = -\mathcal{C}_{10\mu}^V$	(-0.14, -0.02)
	$\mathcal{C}_9^U$	(-1.27, -0.91)

**Table 5.** Allowed  $1\sigma$  parametric space of  $D > 1$  universal and non-universal NP scenarios. These scenarios from S5 to S8 are introduced in [1].

F-II Solutions	Wilson Coefficients	$1\sigma$ range
S9	$\mathcal{C}_{9\mu}^V = -\mathcal{C}_{10\mu}^V$	(-0.29, -0.13)
	$\mathcal{C}_{10}^U$	(-0.23, 0.11)
S10	$\mathcal{C}_{9\mu}^V$	(-0.81, -0.50)
	$\mathcal{C}_{10}^U$	(-0.08, 0.18)
S11	$\mathcal{C}_{9\mu}^V$	(-0.84, -0.52)
	$\mathcal{C}_{10}^U$	(-0.15, 0.09)
S13	$\mathcal{C}_{9\mu}^V$	(-0.97, -0.60)
	$\mathcal{C}_{9\mu}^V$	(0.10, 0.57)
	$\mathcal{C}_{10}^U$	(-0.04, 0.26)
	$\mathcal{C}_{10}^U$	(-0.03, 0.30)

**Table 6.** Allowed  $1\sigma$  parametric space of  $D > 1$  universal and non-universal NP scenarios. The S9 scenario is inspired by 2HDMs [121], scenarios S10 to S13 are inspired by the  $Z'$  model, and vector-like quarks [122] that are introduced in [1].

By using the formulae of observables defined in section §2, we have found the expressions of these observables in terms of NP WCs by integrating over the low  $q^2$  bin for muon and high  $q^2$  bins both for the muon and tauon as the final state leptons which read as follows:

$$\begin{aligned}
10^7 \times \mathcal{B}_r^{[14, s_{max}]}(B_c \rightarrow D_s^* \tau^+ \tau^-) = \\
0.69_{-0.07}^{+0.08} + 0.02_{-0.00}^{+0.00} \{ (C_9^U)^2 + (C_9^U)^2 \} + 0.01_{-0.00}^{+0.00} \{ C_{10}^U C_9^U - C_{10}^U C_9^U - C_{10}^U C_9^U \} \\
- 0.04_{-0.00}^{+0.00} C_9^U C_9^U + 0.09_{-0.01}^{+0.01} \{ C_{10}^U + C_{10}^U \} - 0.23_{-0.02}^{+0.02} C_9^U + 0.25_{-0.03}^{+0.03} C_9^U. \quad (3.2)
\end{aligned}$$

$$\begin{aligned}
10^8 \times \mathcal{B}_r^{[s_{min},6]}(B_c \rightarrow D_s^* \mu^+ \mu^-) = \\
0.97_{-0.01}^{+0.01} + 0.02_{-0.00}^{+0.00} \{ (C_{10}^U)^2 + (C_{10}^V)^2 + (C_9^V)^2 + (C_9^U)^2 + (C_9^U)^2 + (C_{10}^U)^2 + (C_{10}^V)^2 \\
+ (C_9^V)^2 \} + 0.03_{-0.00}^{+0.00} \{ C_{10}^V C_9^U + C_{10}^V C_9^V - C_{10}^U C_{10}^U - C_{10}^U C_{10}^V - C_{10}^U C_9^U - C_{10}^U C_9^V \\
- C_{10}^V C_{10}^U - C_{10}^V C_{10}^V - C_{10}^V C_9^U - C_{10}^V C_9^V + C_{10}^U C_9^U + C_{10}^U C_9^V + C_{10}^U C_9^U + C_{10}^U C_9^V \\
- C_{10}^U C_9^U - C_{10}^U C_9^V + C_{10}^V C_9^U + C_{10}^V C_9^V - C_{10}^V C_9^U - C_{10}^V C_9^V - C_{10}^U C_9^U - C_{10}^U C_9^V \\
- C_9^V C_9^U - C_9^V C_9^V \} + 0.04_{-0.00}^{+0.00} \{ C_{10}^U C_{10}^V + C_{10}^U C_{10}^V + C_9^U C_9^V + C_9^U C_9^V \} \\
+ 0.18_{-0.00}^{+0.00} \{ C_{10}^U + C_{10}^V \} + 0.25_{-0.00}^{+0.00} \{ C_9^V - C_{10}^U - C_{10}^V + C_9^U \} + 0.22_{-0.00}^{+0.00} \{ -C_9^U - C_9^V \}.
\end{aligned} \tag{3.3}$$

$$\begin{aligned}
10^7 \times \mathcal{B}_r^{[14,s_{max}]}(B_c \rightarrow D_s^* \mu^+ \mu^-) = \\
2.86_{-0.32}^{+0.34} + 0.04_{-0.01}^{+0.01} \{ (C_{10}^U)^2 + (C_{10}^V)^2 + (C_{10}^U)^2 + (C_{10}^V)^2 + (C_9^U)^2 + (C_9^V)^2 + (C_9^U)^2 \\
+ (C_9^V)^2 \} + 0.08_{-0.01}^{+0.01} \{ C_{10}^U C_9^U - C_{10}^U C_9^U - C_{10}^V C_9^U + C_{10}^V C_9^U - C_{10}^U C_9^V - C_{10}^V C_9^V \\
+ C_{10}^U C_9^V + C_{10}^V C_9^V + C_{10}^U C_9^U + C_{10}^V C_9^U - C_{10}^U C_9^U - C_{10}^V C_9^U - C_{10}^U C_9^U + C_{10}^U C_9^V \\
+ C_{10}^V C_9^V - C_{10}^U C_9^V - C_{10}^V C_9^V \} + 0.09_{-0.01}^{+0.01} \{ C_{10}^U C_{10}^V - C_{10}^U C_{10}^V - C_{10}^V C_{10}^V + C_{10}^U C_{10}^V \\
- C_9^U C_9^U - C_9^V C_9^U - C_9^U C_9^V - C_9^V C_9^V - C_{10}^U C_{10}^U - C_{10}^V C_{10}^U \} + 0.10_{-0.01}^{+0.01} \{ C_9^U C_9^U \\
+ C_9^U C_9^V \} + 0.69_{-0.07}^{+0.08} \{ C_{10}^U + C_{10}^V - C_9^U - C_{10}^U - C_9^V \} + 0.72_{-0.08}^{+0.09} \{ -C_{10}^U - C_{10}^V \\
+ C_9^U + C_9^V \}.
\end{aligned} \tag{3.4}$$

$$\begin{aligned}
10 \times \mathcal{A}_{FB}^{[14,s_{max}]}(B_c \rightarrow D_s^* \mu^+ \mu^-) = \\
0.85 + 0.01 \{ C_{10}^U - (C_{10}^V)^2 - (C_{10}^V)^2 - (C_9^U)^2 - (C_9^V)^2 - (C_{10}^U)^2 - (C_{10}^V)^2 + C_{10}^V \\
- (C_9^U)^2 - (C_9^V)^2 \} + 0.02 \{ C_{10}^U C_{10}^U + C_{10}^U C_{10}^V - C_{10}^U C_9^U - C_{10}^U C_9^V + C_{10}^V C_{10}^U \\
+ C_{10}^V C_{10}^V - C_{10}^V C_9^U - C_{10}^V C_9^V + C_9^U C_9^U + C_9^V C_9^V - C_{10}^V C_9^U - C_{10}^V C_9^V + C_9^U \\
+ C_9^V - C_{10}^U C_9^U - C_{10}^U C_9^V + C_9^U C_9^U + C_9^U C_9^V \} + 0.03 \{ -C_{10}^U C_{10}^V - C_{10}^U C_{10}^V \\
- C_{10}^U C_9^U - C_{10}^U C_9^V - C_{10}^V C_9^U - C_{10}^V C_9^V - C_9^U C_9^U - C_9^U C_9^V \} + 0.08 \{ C_{10}^U C_9^U \\
+ C_{10}^U C_9^V + C_{10}^V C_9^U + C_{10}^V C_9^V \} + 0.20 \{ -C_{10}^U - C_{10}^V + C_9^U + C_9^V \}.
\end{aligned} \tag{3.5}$$

$$\begin{aligned}
10 \times \mathcal{A}_{FB}^{[s_{min},6]}(B_c \rightarrow D_s^* \mu^+ \mu^-) = \\
-0.66 + 0.02 \{ (C_{10}^U)^2 + (C_{10}^V)^2 + (C_{10}^V)^2 + (C_9^U)^2 + (C_9^U)^2 + (C_9^V)^2 + (C_{10}^U)^2 \\
+ (C_9^V)^2 \} + 0.03 \{ C_{10}^U C_9^U + C_{10}^U C_9^V + C_{10}^V C_9^V + 0.11 C_{10}^V + C_{10}^V C_9^U + C_{10}^V C_9^V \\
+ C_{10}^U C_9^U + C_{10}^U C_9^V + C_{10}^V C_9^U \} + 0.04 \{ -C_{10}^U C_{10}^U - C_{10}^U C_{10}^V - C_9^U C_9^U - C_9^V C_9^U \\
- C_9^V C_9^V - C_9^U C_9^U - C_{10}^V C_{10}^U - C_{10}^V C_{10}^V \} + 0.05 \{ C_{10}^U C_{10}^V + C_{10}^U C_{10}^V + C_9^U C_9^V \\
+ C_9^U C_9^V \} + 0.19 \{ C_{10}^U + C_{10}^V - C_9^U - C_9^V \} + 0.20 \{ C_{10}^U C_9^U + C_{10}^U C_9^V + C_{10}^V C_9^V \\
+ C_{10}^V C_9^U \} - 0.28 \{ C_{10}^U C_9^U - C_{10}^U C_9^V - C_{10}^V C_9^U - C_{10}^V C_9^V \} + 0.11 C_{10}^U \\
+ 1.06 \{ C_9^U + C_9^V \}.
\end{aligned} \tag{3.6}$$

$$\begin{aligned}
10 \times \mathcal{A}_{FB}^{[14, s_{max}]}(B_c \rightarrow D_s^* \tau^+ \tau^-) = \\
0.27 + 0.01 \{ -C_{10}^U C_9^U - (C_9^U)^2 + C_9^U C_9^U - (C_9^U)^2 \} + 0.02 \{ C_{10}^U C_9^U - C_{10}^U \} \\
- 0.03 C_{10}^U + 0.09 C_9^U.
\end{aligned} \tag{3.7}$$

$$\begin{aligned}
10 \times f_L^{[14, s_{max}]}(B_c \rightarrow D_s^* \mu^+ \mu^-) = \\
5.04 + 0.06 \{ (C_{10}^U)^2 + (C_{10}^V)^2 + (C_{10}^V)^2 + (C_9^U)^2 + (C_{10}^U)^2 \} + 0.13 \{ C_{10}^U C_{10}^V \\
+ C_{10}^U C_{10}^V \} + 0.04 \{ C_9^U - C_{10}^V + C_9^V - C_{10}^U \} + 0.08 \{ (C_9^V)^2 + (C_9^U)^2 \\
- C_9^U + (C_9^V)^2 - C_9^V \} + 0.14 \{ C_9^U C_9^V + C_9^U C_9^V \} + 0.10 \{ C_{10}^V + C_{10}^U \} \\
+ 0.15 \{ -C_{10}^U C_{10}^U - C_{10}^U C_{10}^V + C_{10}^U C_9^U + C_{10}^U C_9^V - C_{10}^U C_9^U - C_{10}^U C_9^V \\
- C_{10}^V C_{10}^U - C_{10}^V C_{10}^V + C_{10}^V C_9^U + C_{10}^V C_9^V - C_{10}^V C_9^U - C_{10}^V C_9^V - C_{10}^U C_9^U \\
- C_{10}^U C_9^V + C_{10}^U C_9^U + C_{10}^U C_9^V - C_{10}^V C_9^U - C_{10}^V C_9^V + C_{10}^V C_9^U + C_{10}^V C_9^V \\
- C_9^U C_9^U - C_9^U C_9^V - C_9^V C_9^U - C_9^V C_9^V \}.
\end{aligned} \tag{3.8}$$

$$\begin{aligned}
10 \times f_L^{[s_{min}, 6]}(B_c \rightarrow D_s^* \mu^+ \mu^-) = \\
24 + 0.1 \{ (C_{10}^U)^2 + (C_9^U)^2 + (C_{10}^V)^2 + (C_9^V)^2 + (C_{10}^V)^2 + (C_9^V)^2 + (C_{10}^U)^2 + (C_9^V)^2 \} \\
+ 0.2 \{ C_{10}^U C_{10}^V + C_{10}^U C_{10}^V + C_9^U C_9^V + C_9^U C_9^V \} + 0.7 \{ -C_{10}^U C_{10}^U - C_{10}^U C_{10}^V - C_{10}^V C_{10}^U \\
- C_{10}^V C_{10}^V - C_9^U C_9^U - C_9^U C_9^V - C_9^V C_9^U - C_9^V C_9^V \} + 0.4 \{ -C_9^U - C_9^V \} \\
+ 0.8 \{ C_9^V - C_{10}^U - C_{10}^V + C_9^U \} + 1.1 \{ C_{10}^U C_9^U + C_{10}^U C_9^V - C_{10}^U C_9^U - C_{10}^U C_9^V \\
+ C_{10}^V C_9^U + C_{10}^V C_9^V - C_{10}^V C_9^U - C_{10}^V C_9^V - C_{10}^U C_9^U - C_{10}^U C_9^V + C_{10}^U C_9^U + C_{10}^U C_9^V \\
- C_{10}^V C_9^U - C_{10}^V C_9^V + C_{10}^V C_9^U + C_{10}^V C_9^V \} + 2.7 \{ C_{10}^U + C_{10}^V \}.
\end{aligned} \tag{3.9}$$

$$\begin{aligned}
10 \times \mathcal{A}_{FB}^{[14, s_{max}]}(B_c \rightarrow D_s^* \tau^+ \tau^-) = \\
6.8 + 0.2 \{ C_{10}^U C_9^U - C_{10}^U C_9^U - C_{10}^U C_9^U + C_{10}^U C_9^U + (C_9^U)^2 + (C_9^U)^2 \} - 0.4 \{ C_{10}^U \\
+ C_{10}^U - C_9^U C_9^U + C_9^U \} - 0.8 C_9^U.
\end{aligned} \tag{3.10}$$

Here,  $s_{min} \equiv 4m_\ell^2$  and  $s_{max} \equiv (M_{B_c} - M_{D_s^*})^2$ .

### 3.3 Analysis of the Physical Observables in $B_c \rightarrow D_s^{(*)} \ell^+ \ell^-$ process

Before proceeding to the phenomenological analysis, we describe the legends of the figures, which read as follows: The gray curve is for SM, where the width represents the uncertainty in the SM values due to the form factors. The green, red, and blue bands correspond to the 1D NP scenarios: S1, S2, and S3, respectively. The darker cyan, darker yellow, darker green, magenta, darker blue, pink, orange, and purple bands correspond to the  $D > 1$  NP scenarios: S5, S6, S7, S8, S9, S10, S11, and S13, respectively, where the width of the bands shows the  $1\sigma$  range of the parametric space.

### 3.3.1 1D NP scenarios

In this section, we discuss the impact of 1D NP scenarios on the SM values of the observables under consideration. For this purpose, first, we have calculated the branching ratios of  $B_c \rightarrow D_s^* \ell^+ \ell^-$  ( $\ell = \mu, \tau$ ) and plotted them against the momentum transfer square,  $q^2$ , in Figs.(2a - 2c). These plots show that the branching ratio is an increasing function of  $q^2$  where one can also see that for the case of  $\mu$ , the NP effects become significant in the low  $q^2$  region, after the  $q^2 \geq 2 \text{ GeV}^2$  while for both the  $\mu$  and the  $\tau$  cases, the NP effects are prominent throughout the high  $q^2$  region. However, in the case of  $\mu$  for both low and high  $q^2$  regions, the effects of NP scenarios: S1 and S2 overlap with each other; therefore, the branching ratio of  $B_c \rightarrow D_s^* \mu^+ \mu^-$  is not a suitable observable to distinguish scenarios S1 and S2. In contrast, for the case of  $\tau$ , the effects of scenarios S1, S2, and S3 are pretty distinct from each other, particularly in the  $q^2 = 15 - 17 \text{ GeV}^2$ . Therefore, a precise measurement of the branching ratio  $B_c \rightarrow D_s^* \tau^+ \tau^-$  in this bin provides not only a complementary check of NP but also a better observable to distinguish among the considered 1D NP scenarios, especially to distinguish S1 and S2.

Figs.(2d - 2f) show the forward-backward asymmetry ( $A_{FB}$ ) as a function of  $q^2$ , where it can be noticed that for the case of  $\mu$ , the NP effects are quite prominent and distinguishable from each other in the  $1 \lesssim q^2 \lesssim 1.8 \text{ GeV}^2$  region, on the other hand, in the high  $q^2$  region for both  $\mu$  and  $\tau$  cases, the value of  $A_{FB}$  effects only by the scenarios S1 and S3 while the effects of S2 are negligible. Furthermore, in the low  $q^2$  region for the case of  $\mu$ , all these three scenarios reduce the SM value of  $A_{FB}$  while in the high  $q^2$  region scenario S1 (S3) decreases (increases) and for the case of  $\tau$ , both S1 and S3 increase the value of  $A_{FB}$ . For instance, the maximum increment by the scenario S3 (S2) in the value of  $A_{FB}$  for  $B \rightarrow D^* \tau^+ \tau^-$  is  $\sim 48\%$  ( $\sim 18\%$ ) at  $q^2 \simeq 15 \text{ GeV}^2$ . In contrast, scenario S2 does not affect the value of  $A_{FB}$  throughout the kinematical region for both  $\mu$  and  $\tau$  cases.

In Figs.(2g - 2i), the  $f_L$  is plotted in the low and high  $q^2$  regions, where one can see for the case of  $\mu$  in the low  $q^2$  region, the effects of S3 are quite prominent while the effects of S1 and S2 are mild. Here, we observe that in the presence of S3, the maximum SM value of  $f_L = 0.66$  at  $q^2 \simeq 1.1 \text{ GeV}^2$  not only changed to  $0.86$  at  $q^2 \simeq 1.5 \text{ GeV}^2$  but also this scenario affects its value throughout the  $q^2$  region. However, in the high  $q^2$  region, both S1 and S3 effect the value of  $f_L$  while the effects of S2 are still insignificant. Similarly, for the case of  $\tau$ , the effects of S1 and S3 are significant throughout the  $q^2$  region, especially in the  $13 \lesssim q^2 \lesssim 15 \text{ GeV}^2$  region where the effects are not only prominent but also fairly distinguishable from each other. It is also important to note that at high  $q^2$  region, the effects of S1 and S3 higher the  $f_L$  values for the case of muons while lower the values for the case of tauons throughout the  $q^2$  region.

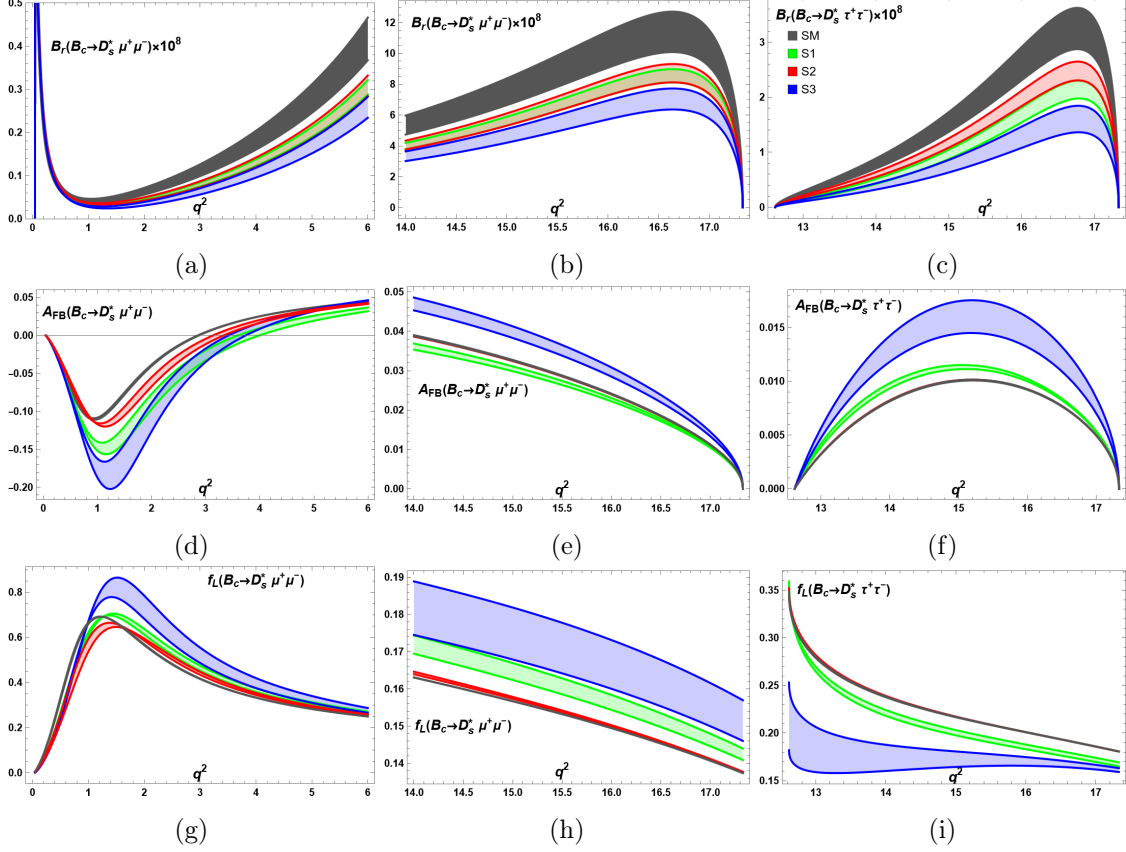


**Figure 2.** (a-c) The branching ratio,  $B_r(B_c \rightarrow D_s^* \ell^+ \ell^-)$  :  $\ell = \mu, \tau$ , (d-f) the forward-backward asymmetry,  $A_{FB}$ , and (g-i) the helicity fraction,  $f_L$ , against the momentum transfer square,  $q^2$ . The gray band is for SM, where the width represents the uncertainty in the SM values due to the form factors. The green, red, and blue bands correspond to the 1D NP scenarios: S1, S2, and S3, respectively, where the width of the bands show the  $1\sigma$  range of the parametric space.

In Fig.(3a), the lepton flavor universality ratio,  $R_{D_s^*}$ , is plotted against  $q^2$  where it can be seen that scenario S2 is overlapped with the SM curve while scenarios S1 and S3 lower the SM values throughout the  $q^2$  region, for instance, one can notice that in scenario S3, the SM value of  $R_{D_s^*} = 0.31$  at  $s_{\max}$  is reduced to 0.24. Moreover, to further complementary check on the LFU, we have also calculated the ratio between the  $A_{FB}$  ( $f_L$ ) when the final state lepton are taus to the  $A_{FB}$  ( $f_L$ ) when the final state lepton are muons, namely,  $R_{A_{FB}}^{\tau\mu} \equiv \frac{A_{FB}(B_c \rightarrow D_s^* \tau^+ \tau^-)}{A_{FB}(B_c \rightarrow D_s^* \mu^+ \mu^-)}$  ( $R_{f_L}^{\tau\mu} \equiv \frac{f_L(B_c \rightarrow D_s^* \tau^+ \tau^-)}{f_L(B_c \rightarrow D_s^* \mu^+ \mu^-)}$ ), respectively. These ratios, in the presence of 1D NP, are plotted as a function of  $q^2$  in Figs.(3b) and (3c).



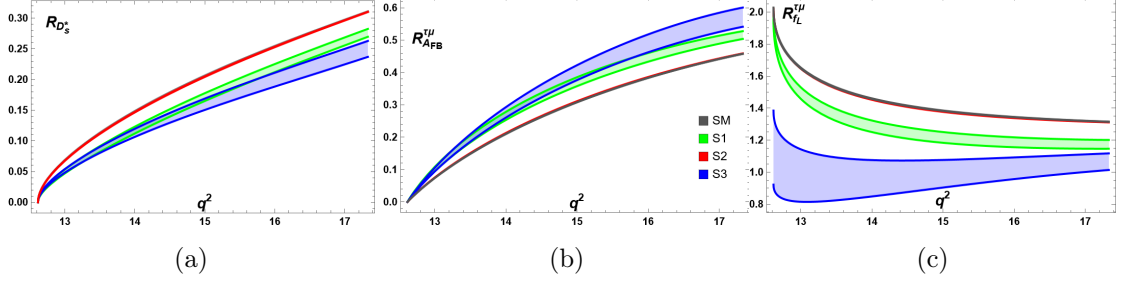


**Figure 3.** (a) The lepton flavor universality ratio,  $R_{D_s^*}$ , (b) the lepton flavor ratio,  $R_{A_{FB}}^{\tau\mu}$ , and (c) the lepton flavor ratio,  $R_{f_L}^{\tau\mu}$ , as a function of  $q^2$  in and beyond the SM scenarios.

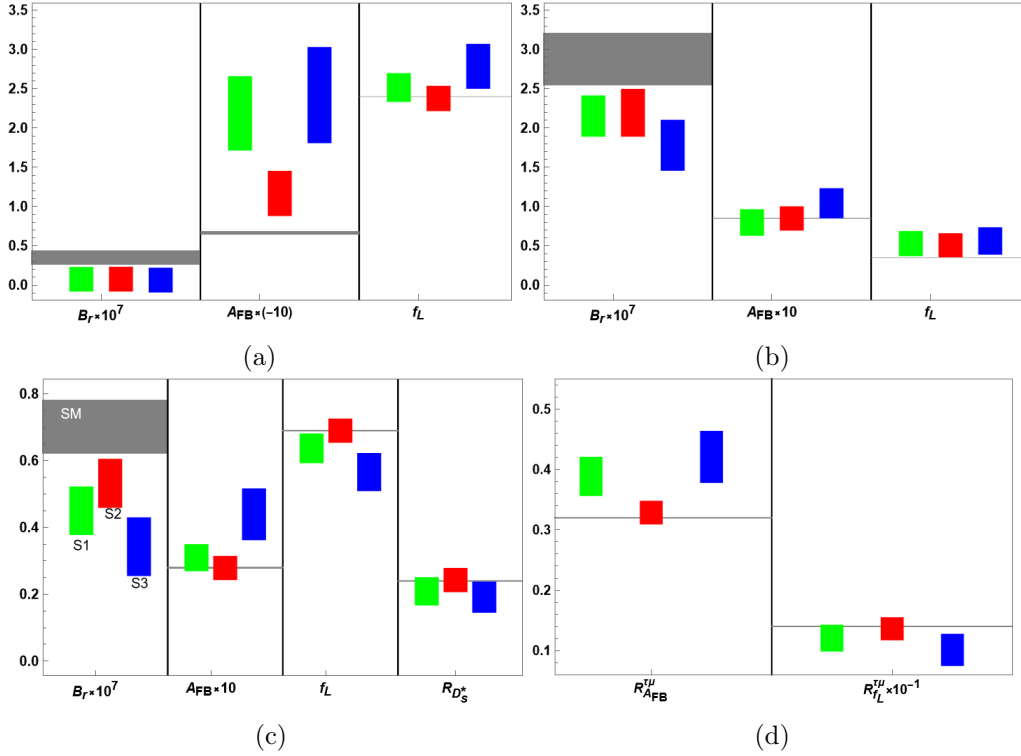


**Figure 4.** The variation in the magnitudes of  $B_r$ ,  $A_{FB}$  and  $f_L$  due to the presence of NP in the (a)  $[s_{min}, 6]$  bin, (b) in the  $[14, s_{max}]$  bin, for the case of muon, and (c) for the case of tauon in  $[14, s_{max}]$  bin while (d) represents the variation in the magnitudes of  $R_{D_s^*}$ ,  $R_{A_{FB}}^{\tau\mu}$  and  $R_{f_L}^{\tau\mu}$ .

In addition, to see the explicit variation in the magnitudes of the observables mentioned above by the considered 1D NP scenarios, we have computed these magnitudes by using the  $1\sigma$  parametric space of NP scenarios after the integration over  $q^2 = s_{min}$  to  $q^2 = 6$  that are shown by the bars in the Fig.(4a) for the muon. Similarly, we also computed these magnitudes by integrating over the region  $q^2 = 14$  to  $q^2 = s_{max}$  for both the muon and tauon which are presented in Figs.(4b) and (4c). The maximum and minimum variation in the magnitude of the ratios in the presence of 1D NP scenarios is also shown by bars in Fig.(4d) computed in  $q^2 = 14$  to  $q^2 = s_{max}$  (high  $q^2$ ). From these bar plots, one can

easily and quantitatively observe the deviation in the SM magnitudes of these observables by considering 1D NP scenarios. Therefore, the precise measurements of these observables, in low and high  $q^2$  bins, not only provide a complementary check to explore the status of the NP but also help to discriminate among the 1D NP scenarios S1, S2, and S3.

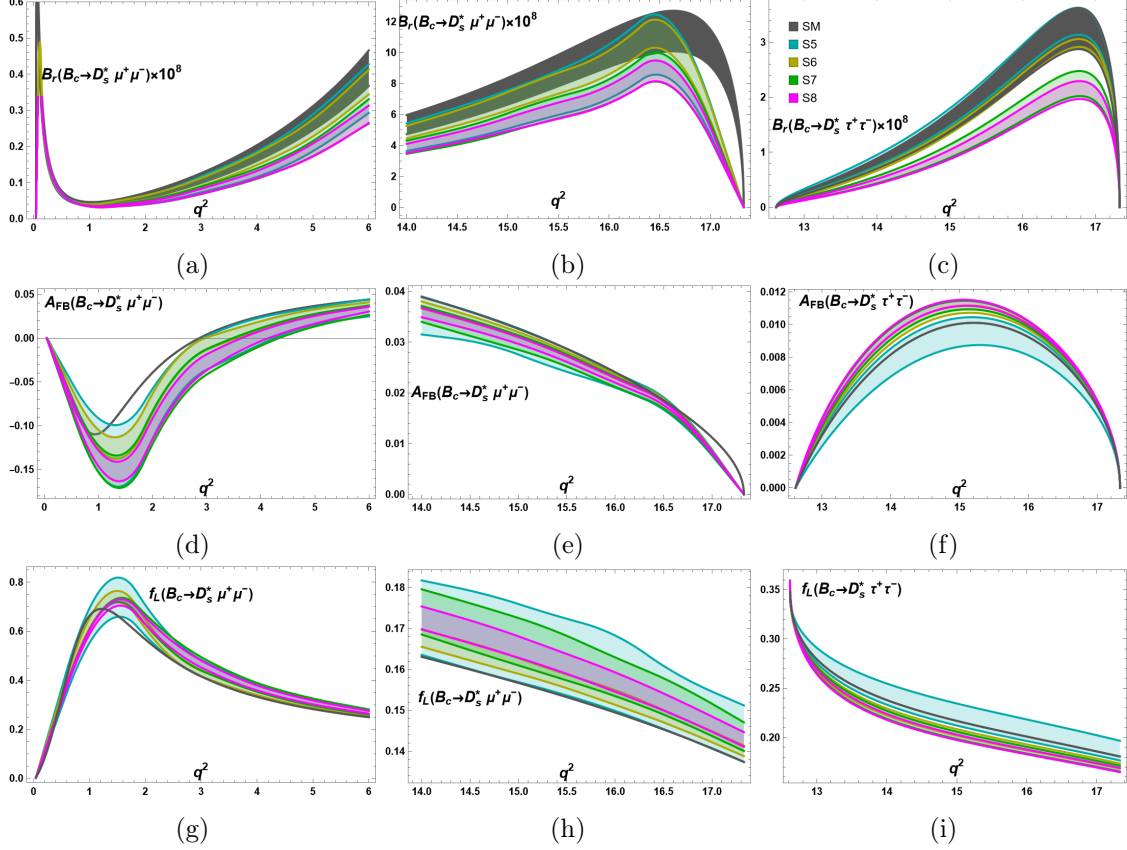


**Figure 5.** (a-c) The  $B_r$ , (d-f) the  $A_{FB}$  and (g-i) the  $f_L$  as a function of  $q^2$ . The gray curve is for the SM, where the width represents the uncertainty in the SM values due to the form factors. The darker cyan, darker yellow, darker green, and magenta bands correspond to the  $D>1$  NP scenarios: S5, S6, S7, and S8, respectively, where the width of the bands show the  $1\sigma$  range of the parametric space.

### 3.3.2 $D>1$ NP scenarios

In Figs. (5a-5c), we have plotted the branching ratio,  $B_r(B_c \rightarrow D_s^* \ell^+ \ell^-)$  where ( $\ell = \mu, \tau$ ) against the  $q^2$  where one can see that for the case of  $\mu$ , the NP effects become significant in the  $q^2 \geq 2 \text{ GeV}^2$  for the scenarios S7 and S8 while S5 and S6 are almost overlapped with the SM. Although the scenarios S7 and S8 effects are prominent and decrease its SM value but overlap with each other. Similar is the case for high  $q^2$  bin both for muon and tauon cases. However, in the case of tauon, the effects of NP scenarios S7 and S8 are more prominent than S5 and S6 effects, which are totally lay in the SM bands.

In Figs. (5d-5f), we have plotted  $A_{FB}$  vs  $q^2$  where we observe that all the four scenarios: S5,  $\dots$ , S8 effect its SM value and at low  $q^2$  for muon, not only change the position of its

minimum value, but also change the position of its zero crossing. On the other hand, at high  $q^2$  for the muon case, all scenarios are destructive and, consequently, lower the  $A_{FB}$  value, while for the tauon case, only S5 lowers the value of SM, and the effects of S6, S7, and S8 are constructive, therefore, increase the value of  $A_{FB}$ .

In Figs. (5g-5i), we have plotted  $f_L$  as a function of  $q^2$ . The trend of NP in this observable both for muon and tauon is opposite to the trend present in  $A_{FB}$ . However, for the muon, the NP effects are comparatively less prominent than  $A_{FB}$  at the low  $q^2$  bin, while in the high  $q^2$  region, these effects are vice versa.

In Figs. (6), we have plotted the considered observables against the  $q^2$  in the presence of those NP scenarios which are motivated by the 2HDM ( $Z'$ ) model(s), namely, S9 (S10, S11, S13). The NP influence in the branching ratio, for the case of muon (see Figs. (6a) and (6b)), are almost the same as the model independent scenarios that are described in Figs. (5a) and (5b). However, for the case of tauon, the effects of scenario S13 are quite distinguishable from the other scenarios as it changes the position of the maximum value of the branching ratio from the high  $q^2 \simeq 17 \text{ GeV}^2$  towards the low value of  $q^2 \simeq 16 \text{ GeV}^2$  (see Fig.5c).

Similarly, in Figs. (6d-6f), we have plotted the  $A_{FB}$  as a function of  $q^2$  where one can see that the NP effects are only prominent for the case of muon in low  $q^2$  bin while in high  $q^2$  region both for the muon and tauon, the effects are mild. It is also important to see here that the effects of scenario S9 are distinguished from the other scenarios (see blue band in Fig. 6d).

Figs. (6g-6i), represent the variation of  $f_L$  in the SM and with NP scenarios as a function of  $q^2$ . From these plots it is obvious to see that the effects are more significant for the case of muon in the high  $q^2$  region except S9. For the case of muon in the low  $1 \lesssim q^2 \lesssim 2$  domain, the effects of NP are mild and overlapped with each other, while for the tauon, only S13 changes the value in the region  $12.6 \lesssim q^2 \lesssim 13.2$ . It is also important to mention here that the effects of S10 and S11 (pink and orange bands) are almost overlapped for all of the observables.

The LFU ratio  $R_{D^*}$  and the ratios:  $R_{A_{FB}}^{\tau\mu}$ ,  $R_{f_L}^{\tau\mu}$  are drawn in Fig. (7) where one can see that the values of these ratios are sensitive to all model-dependent scenarios: S5,  $\dots$ , S8 (see Figs. (7a-7c)) and the scenarios which are motivated by 2HDM and  $Z'$  models: S9 and S10, S11, S13 (see Figss. (7d-7f)). However, for the model-independent scenario, S5 has more prominent and distinguishable effects than the other scenarios. Similarly, the effects of S13, which is motivated by one of the  $Z'$  extension, are more prominent and distinguishable.

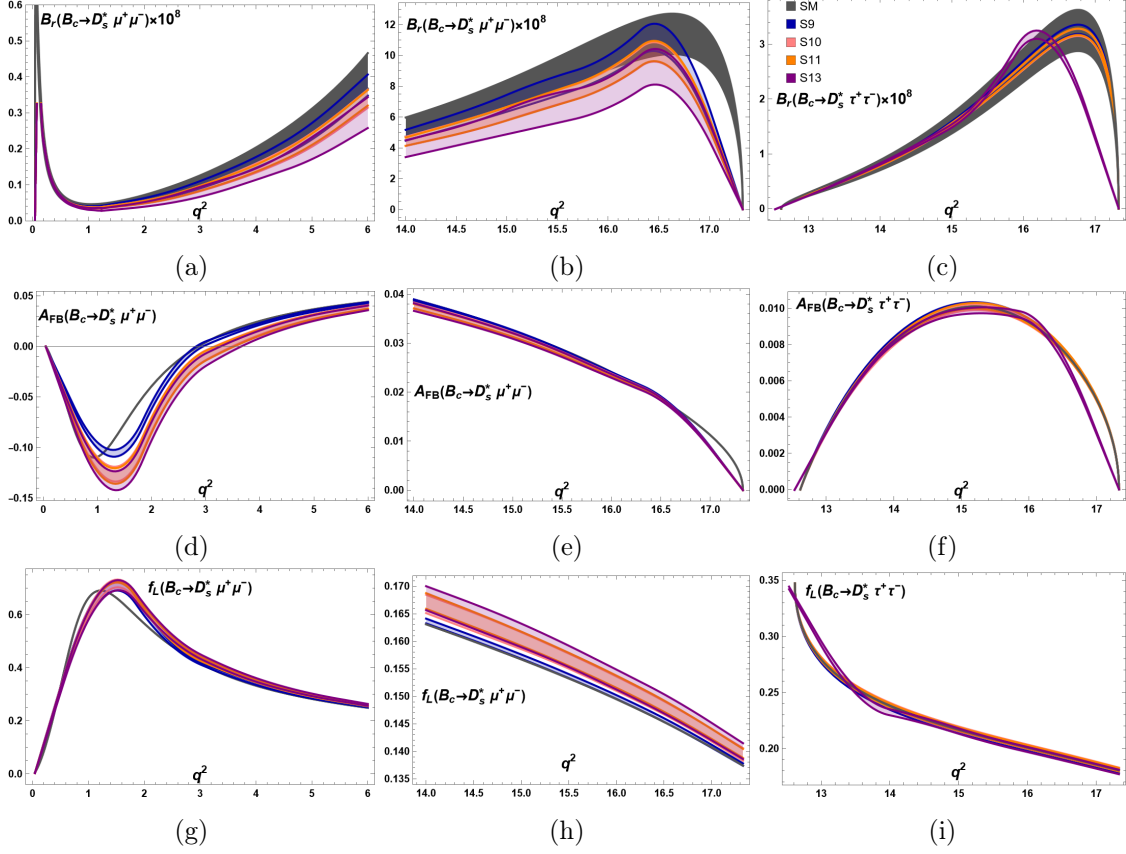


**Figure 6.** (a-c) The  $B_r$ , (d-f) the  $A_{FB}$  and (g-i) the  $f_L$  as a function of  $q^2$ . The gray curve is for the SM, where the width represents the uncertainty in the SM values due to the form factors. The darker blue, pink, orange, and purple bands correspond to the D>1 NP scenarios: S9, S10, S11, and S13, respectively, where the width of the bands show the  $1\sigma$  range of the parametric space.

Similarly, for the 1D NP case, to see the explicit variation in the magnitudes of the observables for D>1 NP case, we have computed the magnitudes of observables by keeping the same configuration as described above for the 1D NP case and drawn them using bar plots in Fig. (8). The first two columns in the first three rows of the figure represent the case of muon in low  $q^2$  region ( $q^2 \in [s_{min}, 6]$ ) and in the high  $q^2$  region ( $q^2 \in [14, s_{max}]$ ), respectively, while the third column represents the case when the final state leptons are tauons. From these bar plots, one can easily and quantitatively observe the variation in the SM magnitudes of these observables by D>1 NP scenarios. Therefore, the precise measurements of these observables, in low and high  $q^2$  bins, not only provide a complementary check to explore the status of the NP but also help to discriminate among the D>1 NP scenarios.

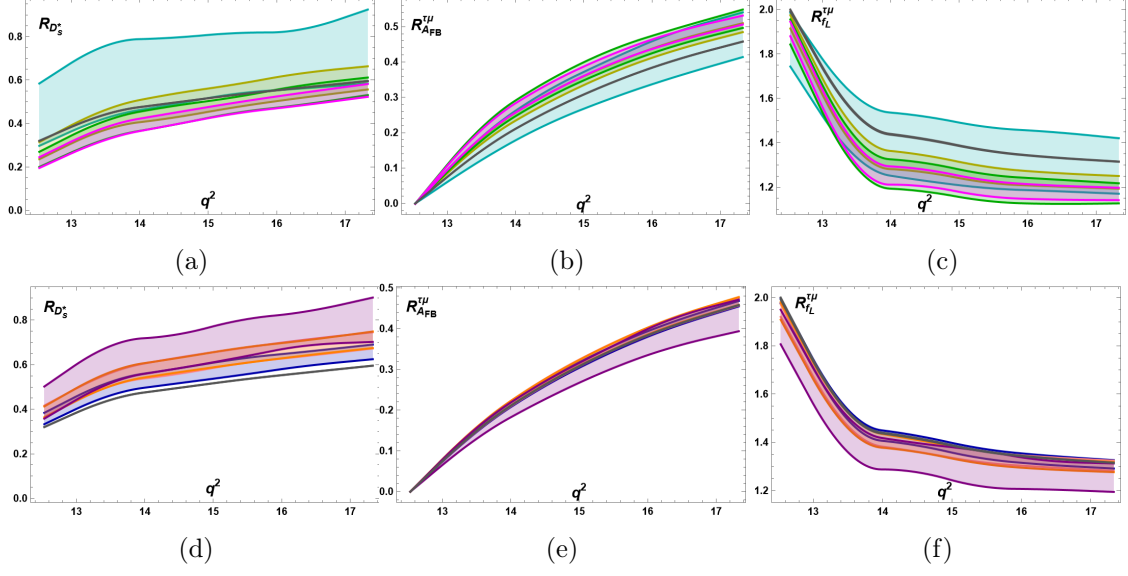


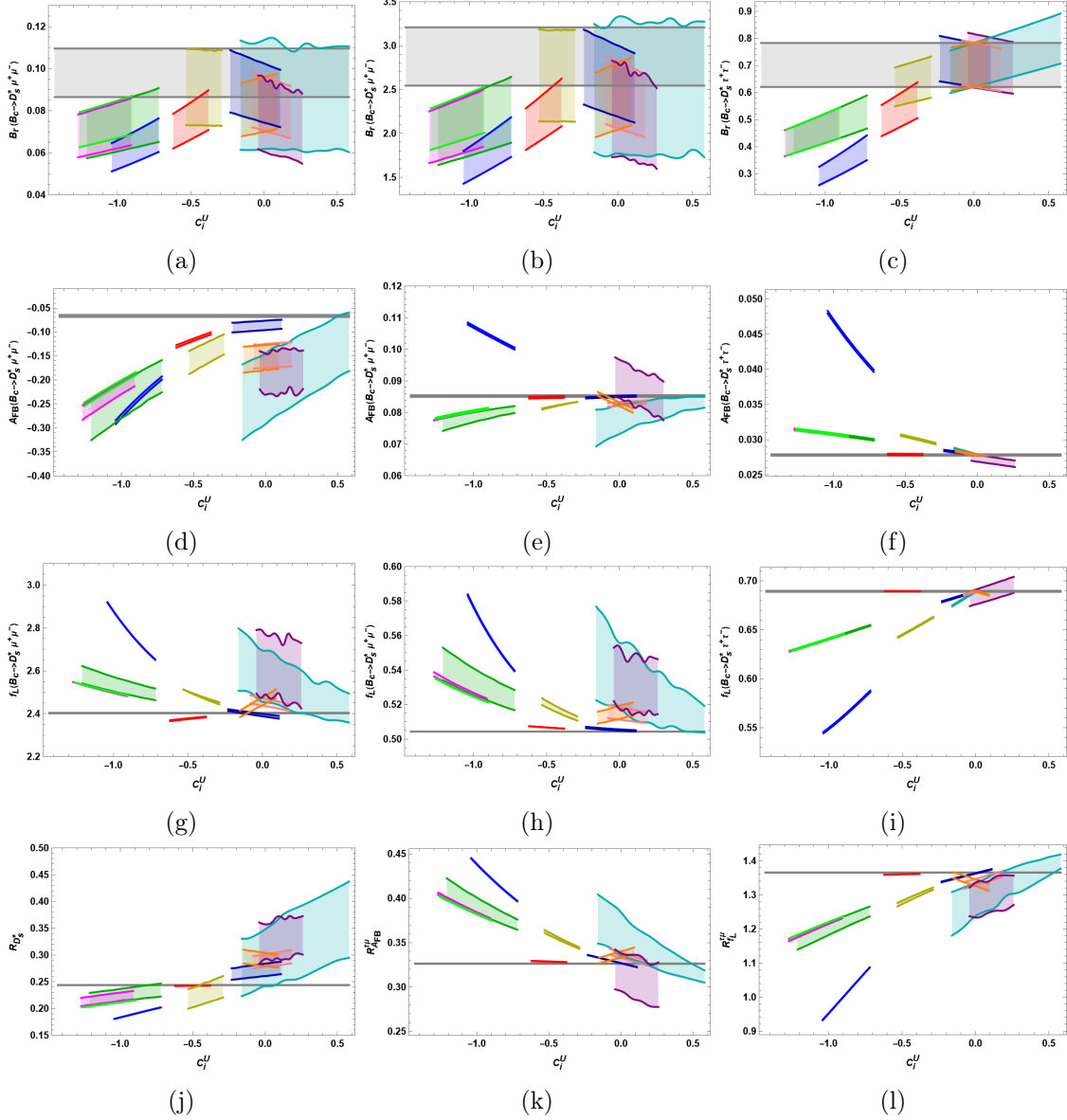
**Figure 7.** The  $R_{D_s^*}$ , the  $R_{AFB}^{\tau\mu}$ , and the  $R_{f_L}^{\tau\mu}$  as a function of  $q^2$  are drawn in (a), (b) and (c), respectively, in the presence of S5, S6, S7 and S8 while (d), (e) and (f) depict the variation of these observables in the presence of S9, S10, S11 and S13.



**Figure 8.** The variation in the magnitudes of  $B_r$ ,  $A_{FB}$ ,  $f_L$  and  $R_{D_s^*}$  due to the presence of  $D > 1$  NP are drawn in (a), (d), (g) and (j), respectively, in the  $[s_{min}, 6]$  bin while (b), (e), (h) and (k) are in the  $[14, s_{max}]$  bin for the case of muon, and (c), (f), (i) and (l) correspond to the case of tauon in  $[14, s_{max}]$ .

Finally, to see the explicit dependence of the observables on the allowed parametric space of the NP WCs, in Fig.(9), we have drawn the observables as a function of NP WCs,  $C_i^{(\prime)j}$ , by integrating over the low and high  $q^2$  bins where  $i = 9, 10, 9\mu, 10\mu$  and  $j = U, V$ . To draw the observables against the  $C_i^{(\prime)j}$ , we have used the expressions defined in Eqs. (3.2-3.10) where we randomly change the values of  $C_{9\mu, 10\mu}^{(\prime)V}$  and make the piece-wise variation in the values of  $C_{9, 10}^{(\prime)U}$  in their  $1\sigma$  ranges that are listed in Tables (4-6). From these plots, one can easily see that how the values of the observables change when we change the values of NP WCs in their allowed  $1\sigma$  parametric space. Consequently, the precise measurement

of these observables may play a pivotal role in not only constraints further the parametric space of the NP scenarios but also provide a deep insight to accommodate the discrepancies present in the  $b \rightarrow s\ell^+\ell^-$  data.



The variation in the magnitudes of  $B_r$ ,  $A_{FB}$ ,  $f_L$  and  $R_{D_s^*}$  as a function of NP WCs are drawn in (a), (d), (g) and (j), respectively, in the  $[s_{min}, 6]$  bin while (b), (e), (h) and (k) are in the  $[14, s_{max}]$  bin for the case of muon, and (c), (f), (i) and (l) correspond to the case of tauon in  $[14, s_{max}]$ .

**Figure 9.** The  $B_r$ ,  $A_{FB}$ ,  $f_L$  and  $R_{D_s^*}$  as a function of NP WCs.

In addition, we have also calculated the numerical values of the observables for  $B_c \rightarrow D_s^* \mu^+(\tau^+) \mu^-(\tau^-)$ , in the SM and in the presence of 1D and D>1 NP scenarios by using

their allowed  $1\sigma$  parametric space, for the low and the high  $q^2$  bins. These values for the case of muons are tabulated in Tables. 7 and 8, and for the case of tauons in Table. 9.

	$10^7 \times \mathcal{B}_r$	$A_{FB}$	$f_L$		$10^7 \times \mathcal{B}_r$	$A_{FB}$	$f_L$
SM	$0.097^{+0.01}_{-0.01}$	$-0.066^{+0.002}_{-0.002}$	$2.402^{+0.001}_{-0.001}$	S7	$(0.064 - 0.080)$	$(-0.16 - -0.31)$	$(2.46 - 2.62)$
S1	$(0.070 - 0.077)$	$(-0.18 - -0.25)$	$(2.48 - 2.54)$	S8	$(0.065 - 0.076)$	$(-0.19 - -0.27)$	$(2.48 - 2.54)$
S2	$(0.070 - 0.079)$	$(-0.10 - -0.13)$	$(2.36 - 2.38)$	S9	$(0.082 - 0.096)$	$(-0.07 - -0.09)$	$(2.38 - 2.41)$
S3	$(0.057 - 0.068)$	$(-0.19 - -0.28)$	$(2.65 - 2.91)$	S10	$(0.075 - 0.087)$	$(-0.12 - -0.17)$	$(2.41 - 2.48)$
S5	$(0.067 - 0.101)$	$(-0.06 - -0.31)$	$(2.36 - 2.78)$	S11	$(0.076 - 0.087)$	$(-0.12 - -0.18)$	$(2.38 - 2.50)$
S6	$(0.082 - 0.097)$	$(-0.10 - -0.18)$	$(2.44 - 2.51)$	S13	$(0.062 - 0.085)$	$(-0.13 - -0.23)$	$(2.43 - 2.82)$

**Table 7.** Observable/ $q^2$  bin (in  $\text{GeV}^2$ ) values  $[s_{min}, 6]$  of different observables of  $B_c \rightarrow D_s^* \mu^+ \mu^-$  decays.

	$10^7 \times \mathcal{B}_r$	$A_{FB}$	$f_L$		$10^7 \times \mathcal{B}_r$	$A_{FB}$	$f_L$
SM	$2.86^{+0.34}_{-0.32}$	$0.085^{+0.0004}_{-0.0004}$	$0.504^{+0.0001}_{-0.0001}$	S7	$(1.85 - 2.35)$	$(0.074 - 0.082)$	$(0.51 - 0.55)$
S1	$(2.04 - 2.26)$	$(0.078 - 0.081)$	$(0.52 - 0.53)$	S8	$(1.87 - 2.22)$	$(0.077 - 0.081)$	$(0.52 - 0.53)$
S2	$(2.04 - 2.34)$	$(0.084 - 0.085)$	$(0.50 - 0.51)$	S9	$(2.40 - 2.83)$	$(0.084 - 0.085)$	$(0.50 - 0.51)$
S3	$(1.60 - 1.95)$	$(0.100 - 0.108)$	$(0.53 - 0.58)$	S10	$(2.20 - 2.57)$	$(0.081 - 0.084)$	$(0.51 - 0.52)$
S5	$(1.95 - 2.96)$	$(0.069 - 0.085)$	$(0.50 - 0.57)$	S11	$(2.20 - 2.56)$	$(0.079 - 0.086)$	$(0.51 - 0.53)$
S6	$(2.40 - 2.84)$	$(0.080 - 0.083)$	$(0.51 - 0.52)$	S13	$(1.78 - 2.51)$	$(0.077 - 0.097)$	$(0.51 - 0.55)$

**Table 8.** Observable/ $q^2$  bin (in  $\text{GeV}^2$ ) values  $[14, s_{max}]$  of different observables of  $B_c \rightarrow D_s^* \mu^+ \mu^-$  decays.



	$10^7 \times \mathcal{B}_r$	$R_{D_s^*}$	$A_{FB}$	$f_L$	$R_{A_{FB}}^{\tau\mu}$	$R_{f_L}^{\tau\mu}$
SM	$0.699^{+0.08}_{-0.07}$	$0.243^{+0.01}_{-0.01}$	$0.027^{+0.00}_{-0.00}$	$0.689^{+0.00}_{-0.00}$	$0.326^{+0.01}_{-0.01}$	$1.366^{+0.01}_{-0.09}$
S1	(0.41 – 0.49)	(0.20 – 0.22)	(0.030 – 0.031)	(0.62 – 0.64)	(0.35 – 0.40)	(1.23 – 1.17)
S2	(0.49 – 0.57)	(0.24 – 0.25)	(0.027 – 0.028)	(0.68 – 0.69)	(0.32 – 0.33)	(1.36 – 1.37)
S3	(0.29 – 0.39)	(0.18 – 0.20)	(0.039 – 0.048)	(0.54 – 0.58)	(0.39 – 0.44)	(0.93 – 1.08)
S5	(0.68 – 0.79)	(0.24 – 0.28)	(0.024 – 0.028)	(0.67 – 0.74)	(0.30 – 0.38)	(1.21 – 1.41)
S6	(0.63 – 0.67)	(0.22 – 0.23)	(0.029 – 0.030)	(0.64 – 0.66)	(0.35 – 0.37)	(1.23 – 1.29)
S7	(0.45 – 0.56)	(0.21 – 0.23)	(0.029 – 0.031)	(0.63 – 0.65)	(0.36 – 0.41)	(1.15 – 1.26)
S8	(0.44 – 0.51)	(0.21 – 0.22)	(0.030 – 0.031)	(0.62 – 0.64)	(0.37 – 0.40)	(1.16 – 1.23)
S9	(0.67 – 0.71)	(0.24 – 0.25)	(0.027 – 0.028)	(0.67 – 0.69)	(0.32 – 0.33)	(1.34 – 1.37)
S10	(0.67 – 0.69)	(0.25 – 0.26)	(0.027 – 0.028)	(0.68 – 0.69)	(0.32 – 0.34)	(1.32 – 1.37)
S11	(0.67 – 0.70)	(0.24 – 0.25)	(0.027 – 0.28)	(0.68 – 0.69)	(0.33 – 0.34)	(1.31 – 1.36)
S13	(0.69 – 0.70)	(0.25 – 0.26)	(0.025 – 0.028)	(0.68 – 0.68)	(0.28 – 0.34)	(1.24 – 1.37)

**Table 9.** Observable/ $q^2$  bin (in  $\text{GeV}^2$ ) values  $[14, s_{max}]$  of different observables of  $B_c \rightarrow D_s^* \tau^+ \tau^-$  decays.

### 3.3.3 $B_c \rightarrow D_s \ell^+ \ell^-$ in the presence of 1D and $D > 1$ NP scenarios

We observe that the branching ratio of the  $B_c \rightarrow D_s \ell^+ \ell^-$  decays are insensitive to the most of the NP scenarios both for the muon and the tauon cases as depicted in Fig. (10).

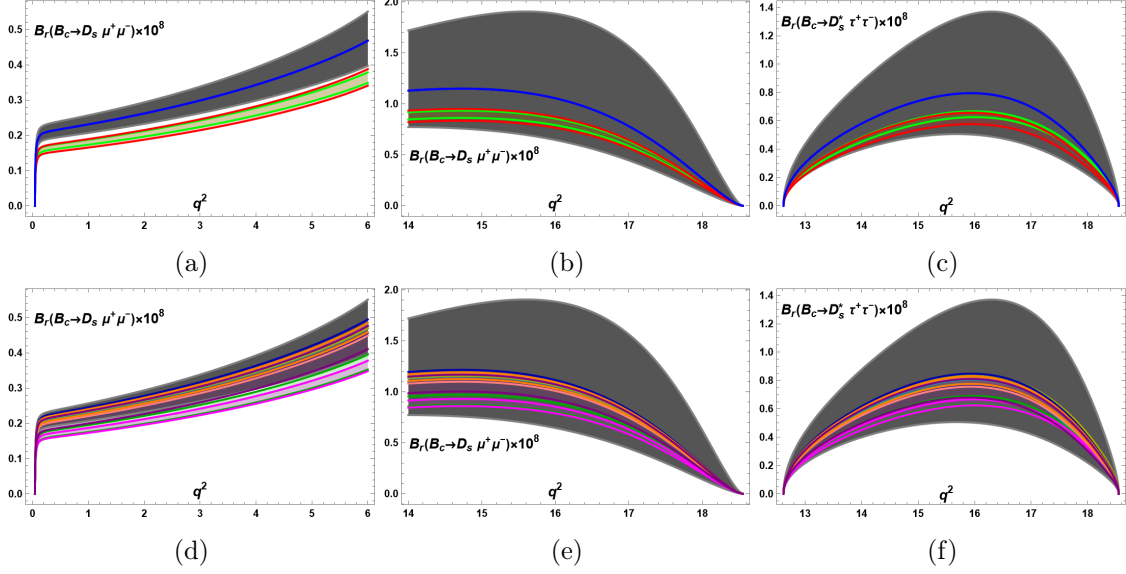


**Figure 10.** The  $B_r$  as a function of  $q^2$  where the plots (a) and (d) represent in  $D=1$  and  $D>1$  NP scenarios, respectively, for the case of muon in the low  $q^2$  region while (b) and (e) represent in the high  $q^2$  region. The plots (c) and (f) represent the case when tauons are the final state leptons.

Except for the scenarios S1, S2, S7 and S8 that have some influence to the value of branching ratio in the low  $q^2$  region for the muon case as can be seen from the Figs. (10a and 10d). However, the LFU ratio,  $R_{D_s}$  is sensitive for the considered NP scenarios as can be seen from Fig. (11). As for  $D=1$  NP scenarios, the value of  $R_{D_s}$  is influenced only by S1 (see Fig. (11a)) which can also be seen explicitly from the variation in the magnitude of its SM value by bar plots that are depicted in Fig. (11c). The influence of  $D>1$  NP scenarios on  $R_{D_s}$  are shown in Fig. (11b) and the variation in the magnitude of the observables are drawn in Fig. (11c). From these figures, one can notice that the effects of S5 are quite prominent from the other scenarios while the effects of other scenarios are overlapped with each other. In addition, we have also drawn the  $R_{D_s}$  as a function of NP WCs in Fig. (11d) where one can explicitly see the effect of  $1\sigma$  allowed parametric space of NP WCs on the observables. In the last, the numerical values of branching ratio and the  $R_{D_s}$  are also listed in Table. (10) This shows that the precise measurement of  $R_{D_s}$  is also a suitable tool for a complementary check on the NP.

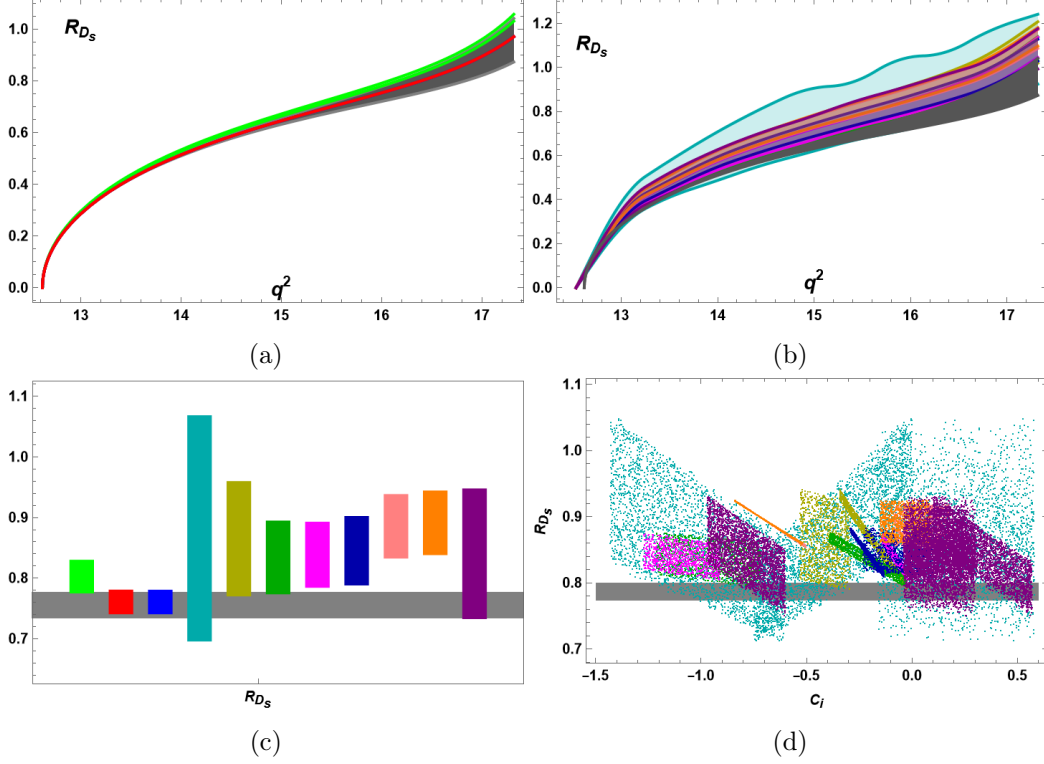


**Figure 11.** (a) and (b) depict  $R_{D_s}$  as a function of  $q^2$  in the presence of  $D=1$  and  $D>1$  NP scenarios, respectively, while (c) represent the variation in the magnitude of  $R_{D_s}$  and (d) correspond to its variation on the allowed  $1\sigma$  parametric space of NP WCs.

	$10^7 \times \mathcal{B}_r$	$R_{D_s}$		$10^7 \times \mathcal{B}_r$	$R_{D_s}$
SM	$1.85^{+0.25}_{-0.25}$	$0.760^{+0.01}_{-0.02}$	S7	$(1.39 - 1.56)$	$(0.79 - 0.87)$
S1	$(1.38 - 1.49)$	$(0.79 - 0.81)$	S8	$(1.38 - 1.49)$	$(0.80 - 0.87)$
S2	$(1.33 - 1.52)$	$(0.75 - 0.77)$	S9	$(1.80 - 1.96)$	$(0.80 - 0.88)$
S3	$(1.85 - 1.86)$	$(0.76 - 0.77)$	S10	$(1.80 - 0.29)$	$(0.85 - 0.91)$
S5	$1.85 - 0.29)$	$(0.71 - 1.04)$	S11	$(1.80 - 1.92)$	$(0.85 - 0.92)$
S6	$(1.86 - 1.89)$	$(0.79 - 0.93)$	S13	$(1.60 - 1.88)$	$(0.75 - 0.92)$

**Table 10.** Observable/ $q^2$  bin (in  $\text{GeV}^2$ ) values  $[14, s_{max}]$  of different observables of  $B_c \rightarrow D_s \tau^+ \tau^-$  decays.

#### 4 Summary and Conclusion

We investigate the transition  $b \rightarrow s \ell^+ \ell^-$  through  $B_c \rightarrow D_s^{(*)} \ell^+ \ell^-$  ( $\ell = \mu, \tau$ ) in different observables by considering the potential NP contribution to  $b \rightarrow s \ell^+ \ell^-$  consisting of universal and non-universal leptons couplings. In our study, we investigate several observables

associated with  $B_c \rightarrow D_s^{(*)} \ell^+ \ell^-$  to check the potential of physics beyond the SM, i.e., the NP.

For this purpose, we use the helicity formalism for this decay by employing the effective theory approach where the vector and axial vector new physics (NP) operators are present. In this study, we have calculated several observables, such as the branching ratio  $B_r$ , the  $D^*$  helicity fraction  $f_L$ , the lepton forward-backward asymmetry  $A_{FB}$ , and the lepton flavor universality ratio (LFU)  $R_{D_s^*}^{\tau\mu}$ . In addition, to a complimentary check on the LFU, we also calculate the ratio of different observables  $R_i^{\tau\mu}$  where  $i = A_{FB}, f_L$ . We assume that the NP universal coupling is present for both muons and taus, while the non-universal coupling is only present for muons. Regarding these couplings, we imply the latest global fit to the  $b \rightarrow s \ell^+ \ell^-$  data.

It is important to mention here that to check the sensitivity of the NP couplings to the observable as a function of  $q^2$ , we set them by optimizing within their  $1\sigma$  ranges, which give the maximum and minimum deviation from their SM values. We give predictions of some of the mentioned observables within the SM and the various NP scenarios. We found that the considered observables are not only sensitive to the NP but also helpful in distinguishing among the different NP scenarios. Moreover, we have also calculated the maximum and minimum variation after the integration over the low  $q^2$  bin for  $\mu$  and high  $q^2$  bin for both  $\mu$  and  $\tau$ . Besides, to see the explicit dependence on the couplings, we have calculated the analytical expressions of these observables in terms of NP WCs and plotted them against the NP couplings in their  $1\sigma$  range, which is very useful for determining the precise values of the universal and non-universal couplings in the future.

These results can be tested at LHCb, HL-LHC, and FCC-ee, and therefore, the precise measurements of these observables not only deepen our understanding of the  $b \rightarrow s \ell^+ \ell^-$  process, but also provide a complementary check of the status of different NP scenarios.

## References

- [1] M. Algueró, A. Biswas, B. Capdevila, S. Descotes-Genon, J. Matias and M. Novoa-Brunet, *To  $(b)e$  or not to  $(b)e$ : no electrons at LHCb*, *Eur. Phys. J. C* **83** (2023) 648 [[arXiv:2304.07330](#)].
- [2] J. Albrecht, D. van Dyk and C. Langenbruch, *Flavour anomalies in heavy quark decays*, *Prog. Part. Nucl. Phys.* **120** (2021) 103885 [[arXiv:2107.04822](#)].
- [3] D. London and J. Matias, *B Flavour Anomalies: 2021 Theoretical Status Report*, *Ann. Rev. Nucl. Part. Sci.* **72** (2022) 37 [[arXiv:2110.13270](#)].
- [4] CDF collaboration, *Search for the flavor-changing neutral current decays  $B^+ \rightarrow \mu^+ \mu^- K^+$  and  $B^0 \rightarrow \mu^+ \mu^- K^{*0}$* , *Phys. Rev. Lett.* **83** (1999) 3378 [[hep-ex/9905004](#)].
- [5] BABAR collaboration, *Search for  $B^+ \rightarrow K^+ \ell^+ \ell^-$  and  $B^0 \rightarrow K^{*0} \ell^+ \ell^-$  lepton-, in 30th International Conference on High-Energy Physics*, 7, 2000 [[hep-ex/0008059](#)].
- [6] BELLE collaboration, *Observation of the decay  $B \rightarrow K \ell^+ \ell^-$* , *Phys. Rev. Lett.* **88** (2002) 021801 [[hep-ex/0109026](#)].
- [7] BABAR collaboration, *Evidence for the rare decay  $B \rightarrow K^* \ell^+ \ell^-$  and measurement of the  $B \rightarrow K \ell^+ \ell^-$  branching fraction*, *Phys. Rev. Lett.* **91** (2003) 221802 [[hep-ex/0308042](#)].

- [8] BABAR collaboration, *Direct CP, Lepton Flavor and Isospin Asymmetries in the Decays  $B \rightarrow K^{(*)}\ell^+\ell^-$* , *Phys. Rev. Lett.* **102** (2009) 091803 [[arXiv:0807.4119](#)].
- [9] BELLE collaboration, *Observation of  $B \rightarrow K^* l^+ l^-$* , *Phys. Rev. Lett.* **91** (2003) 261601 [[hep-ex/0308044](#)].
- [10] BELLE collaboration, *Lepton-Flavor-Dependent Angular Analysis of  $B \rightarrow K^*\ell^+\ell^-$* , *Phys. Rev. Lett.* **118** (2017) 111801 [[arXiv:1612.05014](#)].
- [11] BELLE collaboration, *Test of lepton flavor universality and search for lepton flavor violation in  $B \rightarrow K\ell\ell$  decays*, *JHEP* **03** (2021) 105 [[arXiv:1908.01848](#)].
- [12] BELLE collaboration, *Search for the decay  $B^0 \rightarrow K^* 0 \tau^+ \tau^-$  at the Belle experiment*, *Phys. Rev. D* **108** (2023) L011102 [[arXiv:2110.03871](#)].
- [13] BELLE collaboration, *Measurement of the Differential Branching Fraction and Forward-Backward Asymmetry for  $B \rightarrow K^{(*)}\ell^+\ell^-$* , *Phys. Rev. Lett.* **103** (2009) 171801 [[arXiv:0904.0770](#)].
- [14] BELLE collaboration, *Test of Lepton-Flavor Universality in  $B \rightarrow K^*\ell^+\ell^-$  Decays at Belle*, *Phys. Rev. Lett.* **126** (2021) 161801 [[arXiv:1904.02440](#)].
- [15] BABAR collaboration, *Measurement of Branching Fractions and Rate Asymmetries in the Rare Decays  $B \rightarrow K^{(*)}l^+l^-$* , *Phys. Rev. D* **86** (2012) 032012 [[arXiv:1204.3933](#)].
- [16] CDF collaboration, *Observation of the Baryonic Flavor-Changing Neutral Current Decay  $\Lambda_b \rightarrow \Lambda \mu^+ \mu^-$* , *Phys. Rev. Lett.* **107** (2011) 201802 [[arXiv:1107.3753](#)].
- [17] CMS collaboration, *Angular analysis of the decay  $B^0 \rightarrow K^{*0} \mu^+ \mu^-$  from  $pp$  collisions at  $\sqrt{s} = 8$  TeV*, *Phys. Lett. B* **753** (2016) 424 [[arXiv:1507.08126](#)].
- [18] LHCb collaboration, *Test of lepton universality using  $B^+ \rightarrow K^+ \ell^+ \ell^-$  decays*, *Phys. Rev. Lett.* **113** (2014) 151601 [[arXiv:1406.6482](#)].
- [19] LHCb collaboration, *Measurements of the S-wave fraction in  $B^0 \rightarrow K^+ \pi^- \mu^+ \mu^-$  decays and the  $B^0 \rightarrow K^*(892)^0 \mu^+ \mu^-$  differential branching fraction*, *JHEP* **11** (2016) 047 [[arXiv:1606.04731](#)].
- [20] LHCb collaboration, *Test of lepton universality with  $B^0 \rightarrow K^{*0} \ell^+ \ell^-$  decays*, *JHEP* **08** (2017) 055 [[arXiv:1705.05802](#)].
- [21] LHCb collaboration, *Measurement of Form-Factor-Independent Observables in the Decay  $B^0 \rightarrow K^{*0} \mu^+ \mu^-$* , *Phys. Rev. Lett.* **111** (2013) 191801 [[arXiv:1308.1707](#)].
- [22] BELLE, BELLE-II collaboration, *Search for Rare  $b \rightarrow d \ell^+ \ell^-$  Transitions at Belle*, *Phys. Rev. Lett.* **133** (2024) 101804 [[arXiv:2404.08133](#)].
- [23] LHCb collaboration, *Observation of the suppressed decay  $\Lambda_b^0 \rightarrow p \pi^- \mu^+ \mu^-$* , *JHEP* **04** (2017) 029 [[arXiv:1701.08705](#)].
- [24] LHCb collaboration, *First measurement of the differential branching fraction and CP asymmetry of the  $B^\pm \rightarrow \pi^\pm \mu^+ \mu^-$  decay*, *JHEP* **10** (2015) 034 [[arXiv:1509.00414](#)].
- [25] LHCb collaboration, *First observation of the decay  $B^+ \rightarrow \pi^+ \mu^+ \mu^-$* , *JHEP* **12** (2012) 125 [[arXiv:1210.2645](#)].
- [26] LHCb collaboration, *Evidence for the decay  $B_S^0 \rightarrow \bar{K}^{*0} \mu^+ \mu^-$* , *JHEP* **07** (2018) 020 [[arXiv:1804.07167](#)].

- [27] LHCb collaboration, *Measurement of lepton universality parameters in  $B^+ \rightarrow K^+ \ell^+ \ell^-$  and  $B^0 \rightarrow K^{*0} \ell^+ \ell^-$  decays*, *Phys. Rev. D* **108** (2023) 032002 [[arXiv:2212.09153](#)].
- [28] G. Isidori, D. Lancerini, S. Nabeebaccus and R. Zwicky, *QED in  $\bar{B} \rightarrow \bar{K} \ell^+ \ell^-$  LFU ratios: theory versus experiment, a Monte Carlo study*, *JHEP* **10** (2022) 146 [[arXiv:2205.08635](#)].
- [29] LHCb collaboration, *Test of lepton universality in  $b \rightarrow s \ell^+ \ell^-$  decays*, *Phys. Rev. Lett.* **131** (2023) 051803 [[arXiv:2212.09152](#)].
- [30] LHCb collaboration, *Differential branching fractions and isospin asymmetries of  $B \rightarrow K^{(*)} \mu^+ \mu^-$  decays*, *JHEP* **06** (2014) 133 [[arXiv:1403.8044](#)].
- [31] LHCb collaboration, *Branching Fraction Measurements of the Rare  $B_s^0 \rightarrow \phi \mu^+ \mu^-$  and  $B_s^0 \rightarrow f_2'(1525) \mu^+ \mu^-$  Decays*, *Phys. Rev. Lett.* **127** (2021) 151801 [[arXiv:2105.14007](#)].
- [32] LHCb collaboration, *Measurement of CP-Averaged Observables in the  $B^0 \rightarrow K^{*0} \mu^+ \mu^-$  Decay*, *Phys. Rev. Lett.* **125** (2020) 011802 [[arXiv:2003.04831](#)].
- [33] S. Descotes-Genon, J. Matias, M. Ramon and J. Virto, *Implications from clean observables for the binned analysis of  $B \rightarrow K^* \mu^+ \mu^-$  at large recoil*, *JHEP* **01** (2013) 048 [[arXiv:1207.2753](#)].
- [34] M. Artuso, G. Isidori and S. Stone, *New Physics in  $b$  Decays*, World Scientific (5, 2022), [10.1142/12696](#).
- [35] LHCb collaboration, *Tests of lepton universality using  $B^0 \rightarrow K_S^0 \ell^+ \ell^-$  and  $B^+ \rightarrow K^{*+} \ell^+ \ell^-$  decays*, *Phys. Rev. Lett.* **128** (2022) 191802 [[arXiv:2110.09501](#)].
- [36] CMS collaboration, *Test of lepton flavor universality in  $B^\pm \rightarrow K^\pm \mu^+ \mu^-$  and  $B^\pm \rightarrow K^\pm e^+ e^-$  decays in proton-proton collisions at  $\sqrt{s} = 13$  TeV*, *Rept. Prog. Phys.* **87** (2024) 077802 [[arXiv:2401.07090](#)].
- [37] CDF collaboration, *Search for the Decay  $B_s \rightarrow \mu^+ \mu^- \phi$  in  $p\bar{p}$  Collisions at  $\sqrt{s} = 1.8$ -TeV*, *Phys. Rev. D* **65** (2002) 111101.
- [38] CDF collaboration, *Search for the Rare Decays  $B^+ \rightarrow \mu^+ \mu^- K^+$ ,  $B^0 \rightarrow \mu^+ \mu^- K^{*0}(892)$ , and  $B_s^0 \rightarrow \mu^+ \mu^- \phi$  at CDF*, *Phys. Rev. D* **79** (2009) 011104 [[arXiv:0804.3908](#)].
- [39] D0 collaboration, *Search for the rare decay  $B_s^0 \rightarrow \phi \mu^+ \mu^-$  with the D0 detector*, *Phys. Rev. D* **74** (2006) 031107 [[hep-ex/0604015](#)].
- [40] CDF collaboration, *Measurement of the Forward-Backward Asymmetry in the  $B \rightarrow K^{(*)} \mu^+ \mu^-$  Decay and First Observation of the  $B_s^0 \rightarrow \phi \mu^+ \mu^-$  Decay*, *Phys. Rev. Lett.* **106** (2011) 161801 [[arXiv:1101.1028](#)].
- [41] LHCb collaboration, *Differential branching fraction and angular analysis of the decay  $B_s^0 \rightarrow \phi \mu^+ \mu^-$* , *JHEP* **07** (2013) 084 [[arXiv:1305.2168](#)].
- [42] LHCb collaboration, *Angular analysis and differential branching fraction of the decay  $B_s^0 \rightarrow \phi \mu^+ \mu^-$* , *JHEP* **09** (2015) 179 [[arXiv:1506.08777](#)].
- [43] R.R. Horgan, Z. Liu, S. Meinel and M. Wingate, *Rare  $B$  decays using lattice QCD form factors*, *PoS LATTICE2014* (2015) 372 [[arXiv:1501.00367](#)].
- [44] C. Bobeth, G. Hiller and G. Piranishvili, *CP Asymmetries in  $\bar{B} \rightarrow \bar{K}^*(\rightarrow \bar{K} \pi) \bar{\ell} \ell$  and Untagged  $\bar{B}_s$ ,  $B_s \rightarrow \phi(\rightarrow K^+ K^-) \bar{\ell} \ell$  Decays at NLO*, *JHEP* **07** (2008) 106 [[arXiv:0805.2525](#)].
- [45] A. Bharucha, D.M. Straub and R. Zwicky,  *$B \rightarrow V \ell^+ \ell^-$  in the Standard Model from light-cone sum rules*, *JHEP* **08** (2016) 098 [[arXiv:1503.05534](#)].

- [46] J. Gao, C.-D. Lü, Y.-L. Shen, Y.-M. Wang and Y.-B. Wei, *Precision calculations of  $B \rightarrow V$  form factors from soft-collinear effective theory sum rules on the light-cone*, *Phys. Rev. D* **101** (2020) 074035 [[arXiv:1907.11092](#)].
- [47] R.-H. Li, C.-D. Lu and W. Wang, *Transition form factors of  $B$  decays into  $p$ -wave axial-vector mesons in the perturbative QCD approach*, *Phys. Rev. D* **79** (2009) 034014 [[arXiv:0901.0307](#)].
- [48] A. Deandrea and A.D. Polosa, *The Exclusive  $B_s \rightarrow \phi$  muon+ muon- process in a constituent quark model*, *Phys. Rev. D* **64** (2001) 074012 [[hep-ph/0105058](#)].
- [49] S. Dubnička, A.Z. Dubničková, A. Issadykov, M.A. Ivanov, A. Liptaj and S.K. Sakhiyev, *Decay  $B_s \rightarrow \phi \ell^+ \ell^-$  in covariant quark model*, *Phys. Rev. D* **93** (2016) 094022 [[arXiv:1602.07864](#)].
- [50] A. Issadykov,  *$B_s^0 \rightarrow \bar{K}^*(892)^0 \ell^+ \ell^-$  Decay in Covariant Confined Quark Model*, *Phys. Part. Nucl. Lett.* **19** (2022) 460.
- [51] J.A. Bailey et al.,  *$B \rightarrow K l^+ l^-$  Decay Form Factors from Three-Flavor Lattice QCD*, *Phys. Rev. D* **93** (2016) 025026 [[arXiv:1509.06235](#)].
- [52] P. Ball and R. Zwicky,  *$B_{d,s} \rightarrow \rho, \omega, K^*, \phi$  decay form-factors from light-cone sum rules revisited*, *Phys. Rev. D* **71** (2005) 014029 [[hep-ph/0412079](#)].
- [53] Y.-L. Wu, M. Zhong and Y.-B. Zuo,  *$B(s), D(s) \rightarrow \pi, K, \eta, \rho, K^*, \omega, \phi$  Transition Form Factors and Decay Rates with Extraction of the CKM parameters  $|V(ub)|, |V(cs)|, |V(cd)|$* , *Int. J. Mod. Phys. A* **21** (2006) 6125 [[hep-ph/0604007](#)].
- [54] W. Cheng, X.-G. Wu and H.-B. Fu, *Reconsideration of the  $B \rightarrow K^*$  transition form factors within the QCD light-cone sum rules*, *Phys. Rev. D* **95** (2017) 094023 [[arXiv:1703.08677](#)].
- [55] Y.-M. Wang, Y.-B. Wei, Y.-L. Shen and C.-D. Lü, *Perturbative corrections to  $B \rightarrow D$  form factors in QCD*, *JHEP* **06** (2017) 062 [[arXiv:1701.06810](#)].
- [56] C.-D. Lü, Y.-L. Shen, Y.-M. Wang and Y.-B. Wei, *QCD calculations of  $B \rightarrow \pi, K$  form factors with higher-twist corrections*, *JHEP* **01** (2019) 024 [[arXiv:1810.00819](#)].
- [57] J. Gao, T. Huber, Y. Ji, C. Wang, Y.-M. Wang and Y.-B. Wei,  *$B \rightarrow D \ell \nu_\ell$  form factors beyond leading power and extraction of  $|V_{cb}|$  and  $R(D)$* , *JHEP* **05** (2022) 024 [[arXiv:2112.12674](#)].
- [58] B.-Y. Cui, Y.-K. Huang, Y.-L. Shen, C. Wang and Y.-M. Wang, *Precision calculations of  $B_{d,s} \rightarrow \pi, K$  decay form factors in soft-collinear effective theory*, *JHEP* **03** (2023) 140 [[arXiv:2212.11624](#)].
- [59] W. Wang, R.-H. Li and C.-D. Lu, *Radiative charmless  $B(s) \rightarrow V$  gamma and  $B(s) \rightarrow A$  gamma decays in pQCD approach*, [arXiv:0711.0432](#).
- [60] Z.-J. Xiao and X. Liu, *The two-body hadronic decays of  $B_c$  meson in the perturbative QCD approach: A short review*, *Chin. Sci. Bull.* **59** (2014) 3748 [[arXiv:1401.0151](#)].
- [61] S.-P. Jin, X.-Q. Hu and Z.-J. Xiao, *Study of  $B_s \rightarrow K^{(*)} \ell^+ \ell^-$  decays in the PQCD factorization approach with lattice QCD input*, *Phys. Rev. D* **102** (2020) 013001 [[arXiv:2003.12226](#)].
- [62] S.-P. Jin and Z.-J. Xiao, *Study of  $B_s \rightarrow \phi \ell^+ \ell^-$  Decays in the PQCD Factorization Approach with Lattice QCD Input*, *Adv. High Energy Phys.* **2021** (2021) 3840623 [[arXiv:2011.11409](#)].



- [63] N.R. Soni, A. Issadykov, A.N. Gadaria, J.J. Patel and J.N. Pandya, *Rare  $b \rightarrow d$  decays in covariant confined quark model*, *Eur. Phys. J. A* **58** (2022) 39 [[arXiv:2008.07202](#)].
- [64] C.-D. Lu and W. Wang, *Analysis of  $B \rightarrow K_J^*(\rightarrow K\pi)\mu^+\mu^-$  in the higher kaon resonance region*, *Phys. Rev. D* **85** (2012) 034014 [[arXiv:1111.1513](#)].
- [65] M. Ahmady, S. Keller, M. Thibodeau and R. Sandapen, *Reexamination of the rare decay  $B_s \rightarrow \phi\mu^+\mu^-$  using holographic light-front QCD*, *Phys. Rev. D* **100** (2019) 113005 [[arXiv:1910.06829](#)].
- [66] S.-P. Li, X.-Q. Li, Y.-D. Yang and X. Zhang,  *$R_{D^{(*)}}, R_{K^{(*)}}$  and neutrino mass in the 2HDM-III with right-handed neutrinos*, *JHEP* **09** (2018) 149 [[arXiv:1807.08530](#)].
- [67] B. Barman, D. Borah, L. Mukherjee and S. Nandi, *Correlating the anomalous results in  $b \rightarrow s$  decays with inert Higgs doublet dark matter and muon  $(g-2)$* , *Phys. Rev. D* **100** (2019) 115010 [[arXiv:1808.06639](#)].
- [68] L. Delle Rose, S. Khalil, S.J.D. King and S. Moretti,  *$R_K$  and  $R_{K^*}$  in an Aligned 2HDM with Right-Handed Neutrinos*, *Phys. Rev. D* **101** (2020) 115009 [[arXiv:1903.11146](#)].
- [69] A. Ordell, R. Pasechnik, H. Serôdio and F. Nottensteiner, *Classification of anomaly-free 2HDMs with a gauged  $U(1)'$  symmetry*, *Phys. Rev. D* **100** (2019) 115038 [[arXiv:1909.05548](#)].
- [70] C. Marzo, L. Marzola and M. Raidal, *Common explanation to the  $R_{K^{(*)}}, R_{D^{(*)}}$  and  $\epsilon'/\epsilon$  anomalies in a 3HDM+ $\nu_R$  and connections to neutrino physics*, *Phys. Rev. D* **100** (2019) 055031 [[arXiv:1901.08290](#)].
- [71] S. Iguro and Y. Omura, *Status of the semileptonic  $B$  decays and muon  $g-2$  in general 2HDMs with right-handed neutrinos*, *JHEP* **05** (2018) 173 [[arXiv:1802.01732](#)].
- [72] S. Iguro, *Conclusive probe of the charged Higgs solution of  $P5'$  and  $RD^{(*)}$  discrepancies*, *Phys. Rev. D* **107** (2023) 095004 [[arXiv:2302.08935](#)].
- [73] M.J. Aslam, C.-D. Lu and Y.-M. Wang,  *$B \rightarrow K^*(0) l^+ l^-$  decays in supersymmetric theories*, *Phys. Rev. D* **79** (2009) 074007 [[arXiv:0902.0432](#)].
- [74] S. Trifinopoulos,  *$B$ -physics anomalies: The bridge between  $R$ -parity violating supersymmetry and flavored dark matter*, *Phys. Rev. D* **100** (2019) 115022 [[arXiv:1904.12940](#)].
- [75] A. Shaw, *Looking for  $B \rightarrow X_s \ell^+ \ell^-$  in a nonminimal universal extra dimensional model*, *Phys. Rev. D* **99** (2019) 115030 [[arXiv:1903.10302](#)].
- [76] W. Altmannshofer, S. Gori, M. Pospelov and I. Yavin, *Quark flavor transitions in  $L_\mu - L_\tau$  models*, *Phys. Rev. D* **89** (2014) 095033 [[arXiv:1403.1269](#)].
- [77] B. Bhattacharya, A. Datta, D. London and S. Shivashankara, *Simultaneous Explanation of the  $R_K$  and  $R(D^{(*)})$  Puzzles*, *Phys. Lett. B* **742** (2015) 370 [[arXiv:1412.7164](#)].
- [78] A. Crivellin, G. D'Ambrosio and J. Heeck, *Addressing the LHC flavor anomalies with horizontal gauge symmetries*, *Phys. Rev. D* **91** (2015) 075006 [[arXiv:1503.03477](#)].
- [79] A. Falkowski, M. Nardecchia and R. Ziegler, *Lepton Flavor Non-Universality in  $B$ -meson Decays from a  $U(2)$  Flavor Model*, *JHEP* **11** (2015) 173 [[arXiv:1509.01249](#)].
- [80] B. Bhattacharya, A. Datta, J.-P. Gu  vin, D. London and R. Watanabe, *Simultaneous Explanation of the  $R_K$  and  $R_{D^{(*)}}$  Puzzles: a Model Analysis*, *JHEP* **01** (2017) 015 [[arXiv:1609.09078](#)].



- [81] A. Falkowski, S.F. King, E. Perdomo and M. Pierre, *Flavourful  $Z'$  portal for vector-like neutrino Dark Matter and  $R_{K^{(*)}}$* , *JHEP* **08** (2018) 061 [[arXiv:1803.04430](#)].
- [82] S. Dwivedi, D. Kumar Ghosh, A. Falkowski and N. Ghosh, *Associated  $Z'$  production in the flavorful  $U(1)$  scenario for  $R_{K^{(*)}}$* , *Eur. Phys. J. C* **80** (2020) 263 [[arXiv:1908.03031](#)].
- [83] B. Capdevila, A. Crivellin, C.A. Manzari and M. Montull, *Explaining  $b \rightarrow s\ell^+\ell^-$  and the Cabibbo angle anomaly with a vector triplet*, *Phys. Rev. D* **103** (2021) 015032 [[arXiv:2005.13542](#)].
- [84] G. Hiller and M. Schmaltz,  *$R_K$  and future  $b \rightarrow s\ell\ell$  physics beyond the standard model opportunities*, *Phys. Rev. D* **90** (2014) 054014 [[arXiv:1408.1627](#)].
- [85] B. Gripaios, M. Nardecchia and S.A. Renner, *Composite leptoquarks and anomalies in  $B$ -meson decays*, *JHEP* **05** (2015) 006 [[arXiv:1412.1791](#)].
- [86] D. Bečirević and O. Sumensari, *A leptoquark model to accommodate  $R_K^{\text{exp}} < R_K^{\text{SM}}$  and  $R_{K^*}^{\text{exp}} < R_{K^*}^{\text{SM}}$* , *JHEP* **08** (2017) 104 [[arXiv:1704.05835](#)].
- [87] C. Cornella, J. Fuentes-Martin and G. Isidori, *Revisiting the vector leptoquark explanation of the  $B$ -physics anomalies*, *JHEP* **07** (2019) 168 [[arXiv:1903.11517](#)].
- [88] L. Da Rold and F. Lamagna, *A vector leptoquark for the  $B$ -physics anomalies from a composite GUT*, *JHEP* **12** (2019) 112 [[arXiv:1906.11666](#)].
- [89] O. Popov, M.A. Schmidt and G. White,  *$R_2$  as a single leptoquark solution to  $R_{D^{(*)}}$  and  $R_{K^{(*)}}$* , *Phys. Rev. D* **100** (2019) 035028 [[arXiv:1905.06339](#)].
- [90] A. Datta, J.L. Feng, S. Kamali and J. Kumar, *Resolving the  $(g-2)_\mu$  and  $B$  Anomalies with Leptoquarks and a Dark Higgs Boson*, *Phys. Rev. D* **101** (2020) 035010 [[arXiv:1908.08625](#)].
- [91] A. Crivellin, D. Müller and F. Saturnino, *Flavor Phenomenology of the Leptoquark Singlet-Triplet Model*, *JHEP* **06** (2020) 020 [[arXiv:1912.04224](#)].
- [92] S. Iguro, J. Kawamura, S. Okawa and Y. Omura, *TeV-scale vector leptoquark from Pati-Salam unification with vectorlike families*, *Phys. Rev. D* **104** (2021) 075008 [[arXiv:2103.11889](#)].
- [93] Z.-R. Huang, M.A. Paracha, I. Ahmed and C.-D. Lü, *Testing Leptoquark and  $Z'$  Models via  $B \rightarrow K_1(1270, 1400)\mu^+\mu^-$  Decays*, *Phys. Rev. D* **100** (2019) 055038 [[arXiv:1812.03491](#)].
- [94] D. Das, B. Kindra, G. Kumar and N. Mahajan,  *$B \rightarrow K_2^*(1430)\ell^+\ell^-$  distributions at large recoil in the Standard Model and beyond*, *Phys. Rev. D* **99** (2019) 093012 [[arXiv:1812.11803](#)].
- [95] M.K. Mohapatra and A. Giri, *Implications of light  $Z'$  on semileptonic  $B(B_s) \rightarrow TK2^*(1430)(f_2'(1525))\ell^+\ell^-$  decays at large recoil*, *Phys. Rev. D* **104** (2021) 095012 [[arXiv:2109.12382](#)].
- [96] N. Rajeev, N. Sahoo and R. Dutta, *Angular analysis of  $B_s \rightarrow f_2'(1525)(\rightarrow K^+K^-)\mu^+\mu^-$  decays as a probe to lepton flavor universality violation*, *Phys. Rev. D* **103** (2021) 095007 [[arXiv:2009.06213](#)].
- [97] LHCb collaboration, *Measurement of the  $B_c^-$  meson production fraction and asymmetry in 7 and 13 TeV  $pp$  collisions*, *Phys. Rev. D* **100** (2019) 112006 [[arXiv:1910.13404](#)].
- [98] LHCb collaboration, *A search for rare  $B \rightarrow D\mu^+\mu^-$  decays*, *JHEP* **02** (2024) 032 [[arXiv:2308.06162](#)].

- [99] W.-F. Wang, X. Yu, C.-D. Lü and Z.-J. Xiao, *Semileptonic decays  $B_c^+ \rightarrow D_{(s)}^{(*)}(l^+\nu_l, l^+l^-, \nu\bar{\nu})$  in the perturbative QCD approach*, *Phys. Rev. D* **90** (2014) 094018 [[arXiv:1401.0391](#)].
- [100] C.Q. Geng, C.-W. Hwang and C.C. Liu, *Study of rare  $B_c^+ \rightarrow D_{d,s} + \text{lepton anti-lepton}$  decays*, *Phys. Rev. D* **65** (2002) 094037 [[hep-ph/0110376](#)].
- [101] D. Ebert, R.N. Faustov and V.O. Galkin, *Rare Semileptonic Decays of  $B$  and  $B_c$  Mesons in the Relativistic Quark Model*, *Phys. Rev. D* **82** (2010) 034032 [[arXiv:1006.4231](#)].
- [102] K. Azizi, F. Falahati, V. Bashiry and S.M. Zebarjad, *Analysis of the Rare  $B(c) \rightarrow D^*(s,d) l^+ l^-$  Decays in QCD*, *Phys. Rev. D* **77** (2008) 114024 [[arXiv:0806.0583](#)].
- [103] M.A. Ivanov, J.N. Pandya, P. Santorelli and N.R. Soni, *Decay  $B_c^+ \rightarrow D_{(s)}^{(*)+} \ell^+ \ell^-$  within covariant confined quark model*, [arXiv:2404.15085](#).
- [104] U.O. Yilmaz, *Study of  $B_c \rightarrow D_s^* \ell^+ \ell^-$  in Single Universal Extra Dimension*, *Phys. Rev. D* **85** (2012) 115026 [[arXiv:1204.1261](#)].
- [105] P. Maji, S. Mahata, P. Nayek, S. Biswas and S. Sahoo, *Investigation of rare semileptonic  $B_c \rightarrow (D_{s,d}^{(*)}) \mu^+ \mu^-$  decays with non-universal  $Z'$  effect*, *Chin. Phys. C* **44** (2020) 073106 [[arXiv:2003.12272](#)].
- [106] P. Maji, S. Biswas, P. Nayek and S. Sahoo, *Charged Higgs contribution on  $B_c \rightarrow (D_s, D_s^*) l^+ l^-$* , *PTEP* **2020** (2020) 053B07 [[arXiv:2003.07041](#)].
- [107] A. Ahmed, I. Ahmed, M.A. Paracha, M. Junaid, A. Rehman and M.J. Aslam, *Comparative Study of  $B_c \rightarrow D_s^* \ell^+ \ell^-$  Decays in Standard Model and Supersymmetric Models*, **8**, 2011 [[arXiv:1108.1058](#)].
- [108] M.K. Mohapatra, N. Rajeev and R. Dutta, *Combined analysis of  $B_c \rightarrow D_s^{(*)} \mu^+ \mu^-$  and  $B_c \rightarrow D_s^{(*)} \nu \nu^-$  decays within  $Z'$  and leptoquark new physics models*, *Phys. Rev. D* **105** (2022) 115022 [[arXiv:2108.10106](#)].
- [109] R. Dutta, *Model independent analysis of new physics effects on  $B_c \rightarrow (D_s, D_s^*) \mu^+ \mu^-$  decay observables*, *Phys. Rev. D* **100** (2019) 075025 [[arXiv:1906.02412](#)].
- [110] Y.-S. Li and X. Liu, *Angular distribution of the FCNC process  $B_c \rightarrow D_s^* (\rightarrow D_s \pi) \ell^+ \ell^-$* , *Phys. Rev. D* **108** (2023) 093005 [[arXiv:2309.08191](#)].
- [111] M.K. Mohapatra, A.K. Yadav and S. Sahoo, *Signature of (axial)vector operators in  $B_c \rightarrow D_s^{(*)} \mu^+ \mu^-$  decays*, [arXiv:2409.01269](#).
- [112] N.R. Singh Chundawat, *New physics in  $B \rightarrow K^* \tau^+ \tau^-$ : A model independent analysis*, *Phys. Rev. D* **107** (2023) 055004 [[arXiv:2212.01229](#)].
- [113] A. Faessler, T. Gutsche, M.A. Ivanov, J.G. Korner and V.E. Lyubovitskij, *The Exclusive rare decays  $B \rightarrow K(K^*) \bar{\ell} \ell$  and  $B_c \rightarrow D(D^*) \bar{\ell} \ell$  in a relativistic quark model*, *Eur. Phys. J. direct* **4** (2002) 18 [[hep-ph/0205287](#)].
- [114] HPQCD collaboration, *Rare decay  $B \rightarrow K \ell^+ \ell^-$  form factors from lattice QCD*, *Phys. Rev. D* **88** (2013) 054509 [[arXiv:1306.2384](#)].
- [115] PARTICLE DATA GROUP collaboration, *Review of Particle Physics*, *PTEP* **2022** (2022) 083C01.
- [116] W. Altmannshofer, P. Ball, A. Bharucha, A.J. Buras, D.M. Straub and M. Wick, *Symmetries and Asymmetries of  $B \rightarrow K^* \mu^+ \mu^-$  Decays in the Standard Model and Beyond*, *JHEP* **01** (2009) 019 [[arXiv:0811.1214](#)].

- [117] UTFIT collaboration, *The Unitarity Triangle Fit in the Standard Model and Hadronic Parameters from Lattice QCD: A Reappraisal after the Measurements of Delta  $m(s)$  and  $BR(B \rightarrow \tau \nu(\tau))$* , *JHEP* **10** (2006) 081 [[hep-ph/0606167](#)].
- [118] T. Blake, G. Lanfranchi and D.M. Straub, *Rare B Decays as Tests of the Standard Model*, *Prog. Part. Nucl. Phys.* **92** (2017) 50 [[arXiv:1606.00916](#)].
- [119] A.K. Alok, N.R. Singh Chundawat and A. Mandal, *Investigating the potential of  $RK(*)\tau\mu$  to probe lepton flavor universality violation*, *Phys. Lett. B* **847** (2023) 138289 [[arXiv:2303.16606](#)].
- [120] M. Algueró, B. Capdevila, S. Descotes-Genon, J. Matias and M. Novoa-Brunet,  *$b \rightarrow s\ell^+\ell^-$  global fits after  $R_{K_S}$  and  $R_{K^{*+}}$* , *Eur. Phys. J. C* **82** (2022) 326 [[arXiv:2104.08921](#)].
- [121] A. Crivellin, D. Müller and C. Wiegand,  *$b \rightarrow s\ell^+\ell^-$  transitions in two-Higgs-doublet models*, *JHEP* **06** (2019) 119 [[arXiv:1903.10440](#)].
- [122] C. Bobeth, A.J. Buras, A. Celis and M. Jung, *Patterns of Flavour Violation in Models with Vector-Like Quarks*, *JHEP* **04** (2017) 079 [[arXiv:1609.04783](#)].